iScience

CellPress
OPEN ACCESS

Article

HDAC3 promotes macrophage pyroptosis via regulating histone deacetylation in acute lung injury

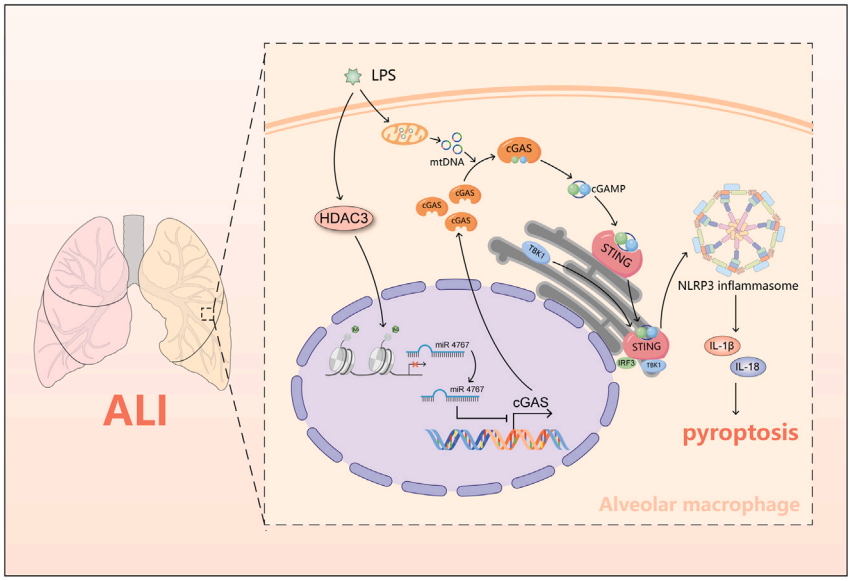

Ning Li, Bohao Liu, Ruyuan He, ..., Chenzhen Xu, Bo Wang, Qing Geng

rmh_wb@whu.edu.cn (B.W.)
gengqingwhu@whu.edu.cn (Q.G.)

Highlights

HDAC3 is abnormally increased in macrophages and aggravates acute lung injury

HDAC3 upregulates pyroptosis in macrophages

HDAC3 regulates cGAS expression through histone deacetylation

Intratracheal instillation of *Hdac3* siRNA-loaded liposomes prevented ALI

Li et al., iScience 26, 107158
July 21, 2023 © 2023
https://doi.org/10.1016/j.isci.2023.107158

iScience

CellPress
OPEN ACCESS

Article

HDAC3 promotes macrophage pyroptosis via regulating histone deacetylation in acute lung injury

Ning Li,[1,3] Bohao Liu,[1,2,3] Ruyuan He,[1] Guorui Li,[1] Rui Xiong,[1] Tinglv Fu,[1] Donghang Li,[1] Chenzhen Xu,[1] Bo Wang,[1,*] and Qing Geng[1,4,*]

SUMMARY

Activated inflammation and pyroptosis in macrophage are closely associated with acute lung injury (ALI). Histone deacetylase 3 (HDAC3) serves as an important enzyme that could repress gene expression by mediating chromatin remodeling. In this study, we found that HDAC3 was highly expressed in lung tissues of lipopolysaccharide (LPS)-treated mice. Lung tissues from macrophage HDAC3-deficient mice stimulated with LPS showed alleviative lung pathological injury and inflammatory response. HDAC3 silencing significantly blocked the activation of cyclic GMP-AMP synthase (cGAS)/stimulator of interferon genes (STING) pathway in LPS-induced macrophage. LPS could recruit HDAC3 and H3K9Ac to the miR-4767 gene promoter, which repressed the expression of miR-4767 to promote the expression of cGAS. Taken together, our findings demonstrated that HDAC3 played a pivotal role in mediating pyroptosis in macrophage and ALI by activating cGAS/STING pathway through its histone deacetylation function. Targeting HDAC3 in macrophage may provide a new therapeutic target for the prevention of LPS-induced ALI.

INTRODUCTION

Acute lung injury (ALI) is a serious clinical pathological condition featured by refractory hypoxemia and progressive dyspnea, which could deteriorate in acute respiratory distress syndrome (ARDS) and multiple organ dysfunction syndrome (MODS) unless treated promptly.[1,2] The most frequent risk factors of ALI and ARDS involve pneumonia, sepsis, near-drowning, inhalation injury, trauma, burn, and drug poisoning.[3] Despite the fact that several advancements has been made over the past few decades, there are still no ideal therapeutic strategies against ALI for the reason that the potential molecular mechanisms driving ALI remain poorly understood. Hence, a more comprehensive understanding of the molecular mechanisms underlying ALI is essential for future treatment of the condition.

Macrophages are the critical cell population in mediating inflammation and tissue damage and serve as a key cellular target for the treatment of ALI.[4] It is reported that the proportion of macrophages in lung immune cells during pulmonary homeostasis is about 90∼95%.[5] There are two types of resident macrophages in lung tissues, namely alveolar macrophages and interstitial macrophages.[6] Under physiologic conditions, alveolar macrophages comprise the first line of defense in innate immune system against microbes and airborne particles.[7] During sepsis-induced ALI, many peripheral macrophages infiltrate into lung tissues and produce various pro-inflammatory cytokines including tumor necrosis factor alpha (TNF-α), interleukin (IL)-1β, and high mobility group box 1(HMGB1). Subsequently, neutrophils from the circulation are recruited into the alveolar spaces and interstitial tissue, giving rise to inflammatory exudation and tissue damage.[6,8] Nod-like receptor protein 3 (NLRP3) inflammasome containing Caspase-1, apoptosis-associated speck-like protein containing a CARD (ASC), and NLRP3 has emerged as an important mediator of inflammatory disease and tissue damage, which is also a promising drug target against ALI.[4] As an intracellular protein complex, NLRP3 inflammasome could be activated by danger signals, environmental stimuli, and various microbes. Then the assembled NLRP3 inflammasome further activates Caspase-1 to trigger gasdermin-meditated pyroptosis by promoting the maturation and production of IL-1β and IL-18 in the cytoplasm, eventually initiating innate immune response.[9] A large number of studies from ourselves and other teams

[1]Department of Thoracic Surgery, Renmin Hospital of Wuhan University, Wuhan 430060, China

[2]Department of Thoracic Surgery, The First Hospital of Jilin University, Changchun 130021, China

[3]The authors contributed equally

[4]Lead contact

*Correspondence: rmh_wb@whu.edu.cn (B.W.), gengqingwhu@whu.edu.cn (Q.G.)

https://doi.org/10.1016/j.isci.2023.107158

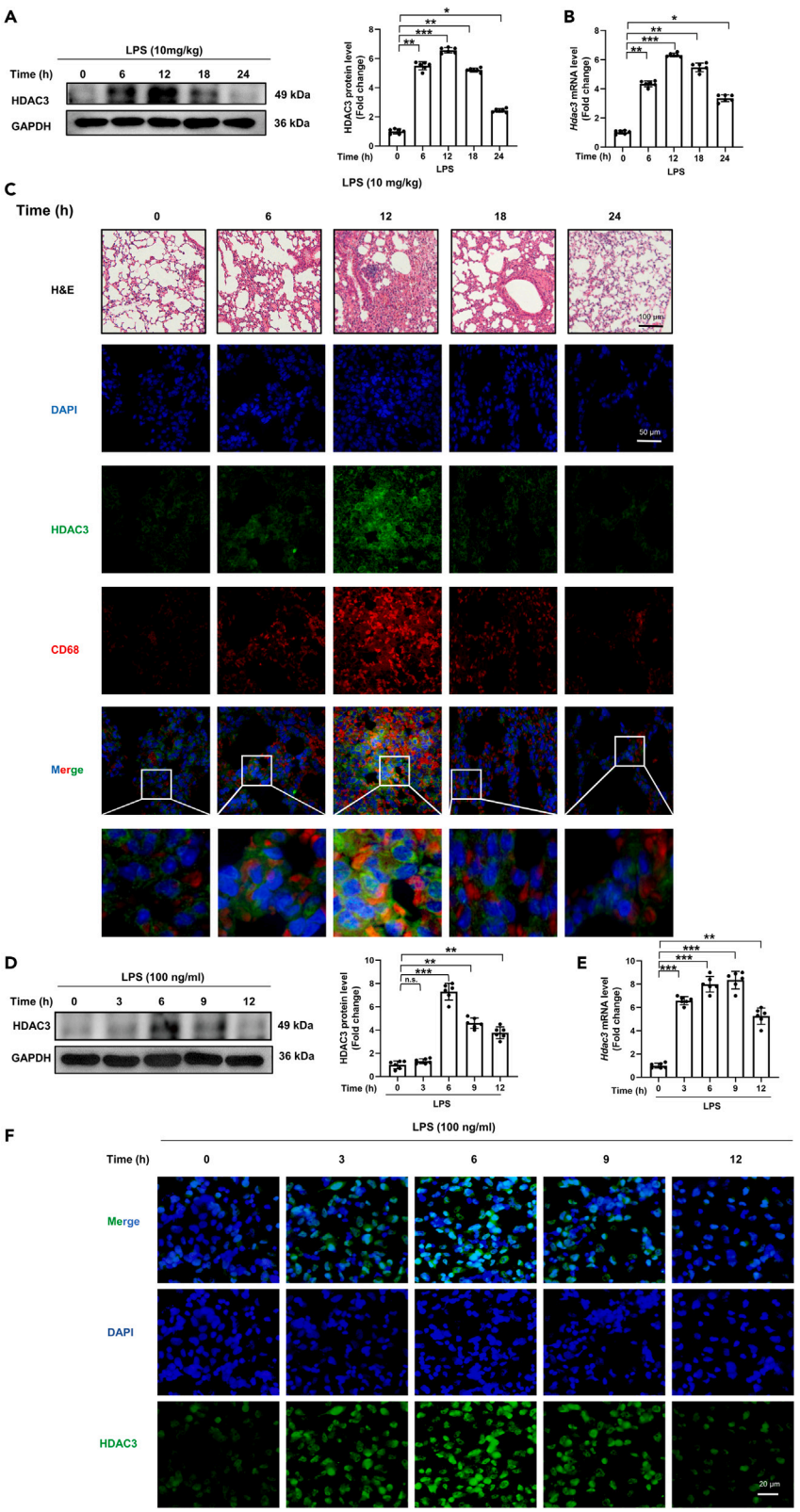
A
LPS (10mg/kg)
Time (h) 0 6 12 18 24
HDAC3
GAPDH
49 kDa
36 kDa
HDAC3 protein level (Fold change)
Time (h) 0 6 12 18 24
LPS
LPS (10 mg/kg)
B
Hdac3 mRNA level (Fold change)
Time (h) 0 6 12 18 24
LPS
C
Time (h)
0 6 12 18 24
H&E
100 μm
DAPI
50 μm
HDAC3
CD68
Merge
D
LPS (100 ng/ml)
Time (h) 0 3 6 9 12
HDAC3
GAPDH
49 kDa
36 kDa
HDAC3 protein level (Fold change)
n.s.
Time (h) 0 3 6 9 12
LPS
E
Hdac3 mRNA level (Fold change)
Time (h) 0 3 6 9 12
LPS
F
LPS (100 ng/ml)
Time (h) 0 3 6 9 12
Merge
DAPI
HDAC3
20 μm

Figure 1. The expression of HDAC3 in lung tissues and differentiated THP-1 cells upon LPS stimulation

(A) Western blot analysis of HDAC3 in the lungs of mice following LPS induction (n = 6).

(B) Relative mRNA levels of HDAC3 in the lung tissues following LPS induction (n = 6).

(C) Representative results for the H&E staining and coimmunostaining of CD68 and HDAC3 in the lung tissues following LPS induction (n = 6). Arrows indicate where the staining overlapped.

(D) Western blot analysis of HDAC3 in differentiated THP-1 cells following LPS induction (100 ng/ml) (n = 6).

(E) Relative mRNA levels of HDAC3 in differentiated THP-1 cells following LPS induction (100 ng/ml) (n = 6).

(F) Immunofluorescence staining of HDAC3 in differentiated THP-1 cells following LPS induction (100 ng/ml) (n = 6).

Values represent the mean ± SEM. *p < *0.05*, **p < *0.01*, ***p < *0.001* versus the matched groups, n.s. represents no significance.

have unveiled that the activation of NLRP3 inflammasome and pyroptosis in macrophage are closely related with the development of ALI.[10–13] Therefore, the inhibition of NLRP3 inflammasome and pyroptosis in macrophages is thought to be important for the prevention and treatment of ALI.

Histones serve as intra-nuclear cationic proteins which are mainly responsible for gene expression through stabilizing chromatin structure in eukaryotic cells, the abnormal acetylation of which is associated with various diseases.[14–17] Histone deacetylases (HDACs) are a class of enzymes that possess the ability to deacetylate not only histones but also a wide range of non-histone proteins in the cytoplasm, nucleus, and mitochondria.[18,19] In recent years, the functions of some HDACs in ALI have been gradually disclosed. For instance, in mice with pneumonia-induced ALI, inhibiting HDAC7 by Trichostatin A could obviously relieve inflammatory injury in lung tissues and improved survival condition.[20] HDAC3 inhibition obviously suppressed the mitochondrial pathway of apoptosis and maintained mitochondrial membrane potential in kidney cold storage/transplantation injury.[21] Additionally, HDAC3 could govern inflammatory responses through its non-canonical deacetylase-independent activity.[22] One recent study also disclosed that HDAC3 inhibition could prevent lipopolysaccharide (LPS)-induced endotoxemia in mice. However, the underlying mechanisms by which HDAC3 functions have not been explored yet.[23] Given the findings above, we speculate that HDAC3 may serve as a novel target for therapeutic intervention in LPS-induced inflammation and ALI.

In the present study, we found that HDAC3 was consistently induced in lung tissues and macrophages of LPS-induced ALI, displaying a significant correlation with pulmonary inflammation and injury. Moreover, HDAC3 deficiency in macrophages significantly alleviated LPS-induced ALI and, meanwhile, reduced pyroptosis of macrophages in murine lung tissues. In terms of mechanisms, HDAC3 could decrease histone acetylation of the miR-4767 gene promoter, by which it promoted the expression of cGAS and pyroptosis in LPS-induced macrophages. Thus, intratracheal administration of liposomes with *Hdac3* small interfering RNAs (siRNAs) could protect against LPS-induced ALI in mice by targeting pyroptosis in macrophage.

RESULTS

HDAC3 was upregulated in lung tissues and macrophages during ALI

To explore the possible involvement of HDAC3 in ALI, we first detected expression levels of HDAC3 in lung tissues from LPS-treated mice. As shown in Figures 1A and 1B, compared with the baseline status, both the protein and mRNA expression levels of HDAC3 were obviously increased in lung tissues from LPS-treated mice. Based on the results of inflammatory cytokines levels in mouse lung tissues, we found that the changes of HDAC3 were synchronized with the inflammatory levels, including IL-18, IL-1β, TNF-α, and HMGB1, which are markers of pyroptosis (Figure S1). According to Figure 1C, we found that the pathological injury of lung tissue was the most serious at 12 h after LPS stimulation, and accompanied by the aggravation of pathological injury, the expression of HDAC3 increased. The immunofluorescent staining further revealed that HDAC3 was significantly increased with the infiltration of macrophages, and the former was significantly co-localized with macrophage marker CD68. (Figure 1C). Additionally, the expression levels of HDAC3 in LPS-treated THP-1 cells were also measured. As shown in Figures 1D and 1E, LPS stimulation significantly increased the protein and mRNA expression levels of HDAC3 in differentiated THP-1 cells. In particular, after LPS stimulation for 6 h, the protein expression level of HDAC3 in macrophages reached a peak. The immunofluorescent staining (Figure 1F) further confirmed the upregulation of HDAC3 in macrophages. These results suggested that HDAC3 might participate in the development of sepsis-induced ALI.

HDAC3 contributed to LPS-induced inflammatory response in macrophages

Next, we evaluated the function of HDAC3 in differentiated THP-1 cells in response to LPS challenge. To begin with, three pairs of siRNA according to the sequences of the HDAC3 mRNA were synthesized

(siRNA1, siRNA2, and siRNA3) and transfected to knock down the expression of HDAC3 in macrophages. Based on the inhibiting efficiency, siRNA2 was selected for subsequent *in vitro* experiments (Figure 2A). To induce pyroptosis in macrophages, the cells were then stimulated with LPS (1 μg/mL) for 4 h, followed by the incubation with nigericin (10 μM) for 0.5 h. The mRNA levels of pro-inflammatory cytokines including *Tnf-α*, *Il-6*, *Ccl-2*, and *Il-1β* were detected. As shown in Figures 2B–2E, downregulating HDAC3 at baseline displayed no effects on inflammatory response in differentiated THP-1 cells. However, in the context of LPS stimulation, HDAC3-knockdown macrophages showed significantly reduced inflammatory response, evidenced by decreased mRNA levels of *Tnf-α*, *Il-6*, *Ccl-2*, and *Il-1β*. Cell viability in differentiated THP-1 cells was also detected. Compared with cell viability in the LPS+si-NC(negative control) group, HDAC3 knockdown markedly improved cell viability in differentiated THP-1 cells challenged with LPS (Figure 2F). Meanwhile, the role of HDAC3 overexpression in differentiated THP-1 cells in response to LPS challenge was also observed. HDAC3-overexpressing macrophages were constructed by infecting with adenovirus (Ad)-Hdac3 (Figure 2G). Similarly, the mRNA levels of pro-inflammatory cytokines as well as cell viability in differentiated THP-1 cells challenged with LPS stimulation were investigated. As expected, HDAC3 overexpression significantly aggravated inflammatory response and further impaired cell viability in differentiated THP-1 cells in response to LPS challenge (Figures 2H–2L). These findings hinted that HDAC3 inhibition prevented LPS-induced inflammation in differentiated THP-1 cells.

HDAC3 deficiency in macrophage alleviated lung pathological injury and inflammation in mice

To further confirm the potential roles of HDAC3 in mice with ALI, we next generated macrophage HDAC3-deficient mice by genetic engineering (Figure 3A), which selectively deleted HDAC3 in macrophages. HDAC3 depletion was verified through genotyping of the toe DNA to prove the presence of the flox allele (Figure S5). The HDAC3 protein expression in lung tissues and primary macrophages from HDAC3-CKO (conditional knockout) mice as well as HDAC3-C mice was confirmed via western blot (Figures 3B and 3C). Significantly attenuated lung pathological injury and decreased lung injury score were noted in HDAC3-CKO mice as illustrated by the H&E staining (Figures 3D and 3E). Additionally, lung wet/dry weight in mice from HDAC3-CKO+LPS group was significantly lower than that in HDAC3-C+LPS group (Figure 3F). Furthermore, we also observed that HDAC3 deficiency in macrophage significantly decreased the mRNA levels of *Il-6*, *Il-1β*, and *Tnf-α* in lung tissues from LPS-treated mice (Figures 3G–3I). And the immunohistochemical staining also showed that HDAC3 deficiency could inhibit the upregulation of IL-6 in lung tissues from mice with ALI (Figure 3J). We also measured the levels of inflammatory cytokines in the bronchial lavage fluid (BALF) of the mice and, not surprisingly, found that HDAC3 deficiency effectively reduced the secretion of inflammatory cytokines (Figure 3K). In summary, our data support that specific loss of HDAC3 in macrophages could prevent mice from LPS-induced lung pathological injury and inflammation.

HDAC3 deficiency inhibited LPS-induced pyroptosis in macrophage

Given the critical roles of NLRP3 inflammasome and pyroptosis played in the development of sepsis-induced ALI, we next detected the extent to which pyroptosis occurs *in vivo* and *in vitro*. Phorbol 12-myristate 13-acetate (PMA)-induced THP-1 cells were transfected with si-NC and si-HDAC3, respectively, and we observed under the microscope that THP-1 cells showed obvious polarization, swelling, and even rupture upon LPS stimulation, which was largely reversed by HDAC3 inhibition (Figure 4A). Based on the above results, we next detected the protein expression as well as other markers of pyroptosis *in vivo* and *in vitro*. Impressively, HDAC3 inhibition significantly decreased the protein levels of NLRP3, Pro-Caspase-1, Caspase-1 p20, and Gasdermin-D (GSDMD)-N in differentiated THP-1 cells in response to LPS challenge (Figure 4B). Propidium Iodide (PI)-Hoechst staining further confirmed that HDAC3 inhibition could suppress LPS-induced pyroptosis in differentiated THP-1 cells (Figure 4C). Additionally, IL-1β and IL-18 in differentiated THP-1 cells were also detected. The results showed that HDAC3 inhibition also decreased the levels of IL-1β and IL-18 in LPS-treated macrophages (Figures 4D and 4E). To further explore possible mechanisms contributing to LPS-induced pyroptosis in macrophage, the GSE140610 from the public database containing transcriptomic information was analyzed. As shown in Figure S2, the differentially expressed genes (DEGs) in bone marrow-derived macrophage (BMDM) between LPS group and LPS+HDAC3-knockout group were mainly enriched in innate immune and cell response to interferon-gamma. Therefore, the innate immune cyclic GMP–AMP synthase (cGAS)/stimulator of interferon genes (STING) pathway in differentiated THP-1 cells was investigated. Western blots showed that LPS stimulation significantly activated cGAS/STING pathway in differentiated THP-1 cells, which could be reversed after HDAC3 was inhibited (Figure 4F). It is worth noting that HDAC3 inhibition at baseline decreases the protein level of cGAS but showed no effects on the phosphorylation of STING, indicating that HDAC3 may affect

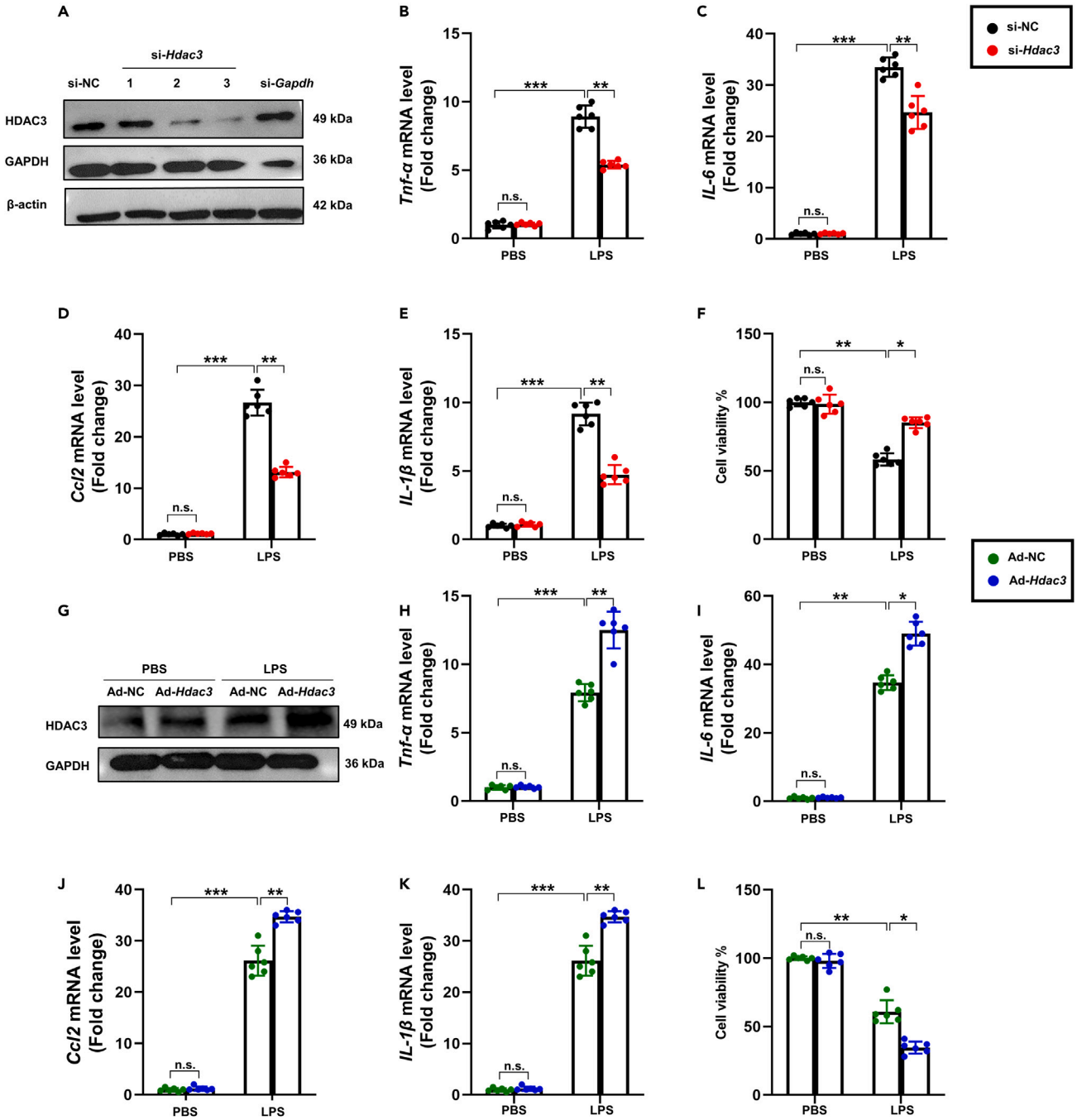

Figure 2. HDAC3 contributed to LPS-induced inflammatory response in macrophages

(A) Western blot analysis of HDAC3 in differentiated THP-1 cells transfected with three pairs of si-*Hdac3* and si-*Gapdh* (n = 6).

(B–E) Relative mRNA levels of Tnf-α, IL-6, Ccl-2, and IL-1β in Hdac3-knockdown THP-1 cells following LPS/nigericin induction (n = 6).

(F) Cell viability in Hdac3-knockdown THP-1 cells following LPS/nigericin induction (n = 6).

(G) Western blot analysis of HDAC3 in differentiated THP-1 cells transduced with Ad-*Hdac3*.

(H–K) Relative mRNA levels of Tnf-α, IL-6, Ccl-2, and IL-1β in Ad-*Hdac3*-transduced THP-1 cells following LPS/nigericin induction (n = 6).

(L) Cell viability in Ad-*Hdac3*-transduced THP-1 cells following LPS/nigericin induction (n = 6). Values represent the mean ± SEM. *p < *0.05*, **p < *0.01*, ***p < *0.001* versus the matched groups, n.s. represents no significance.

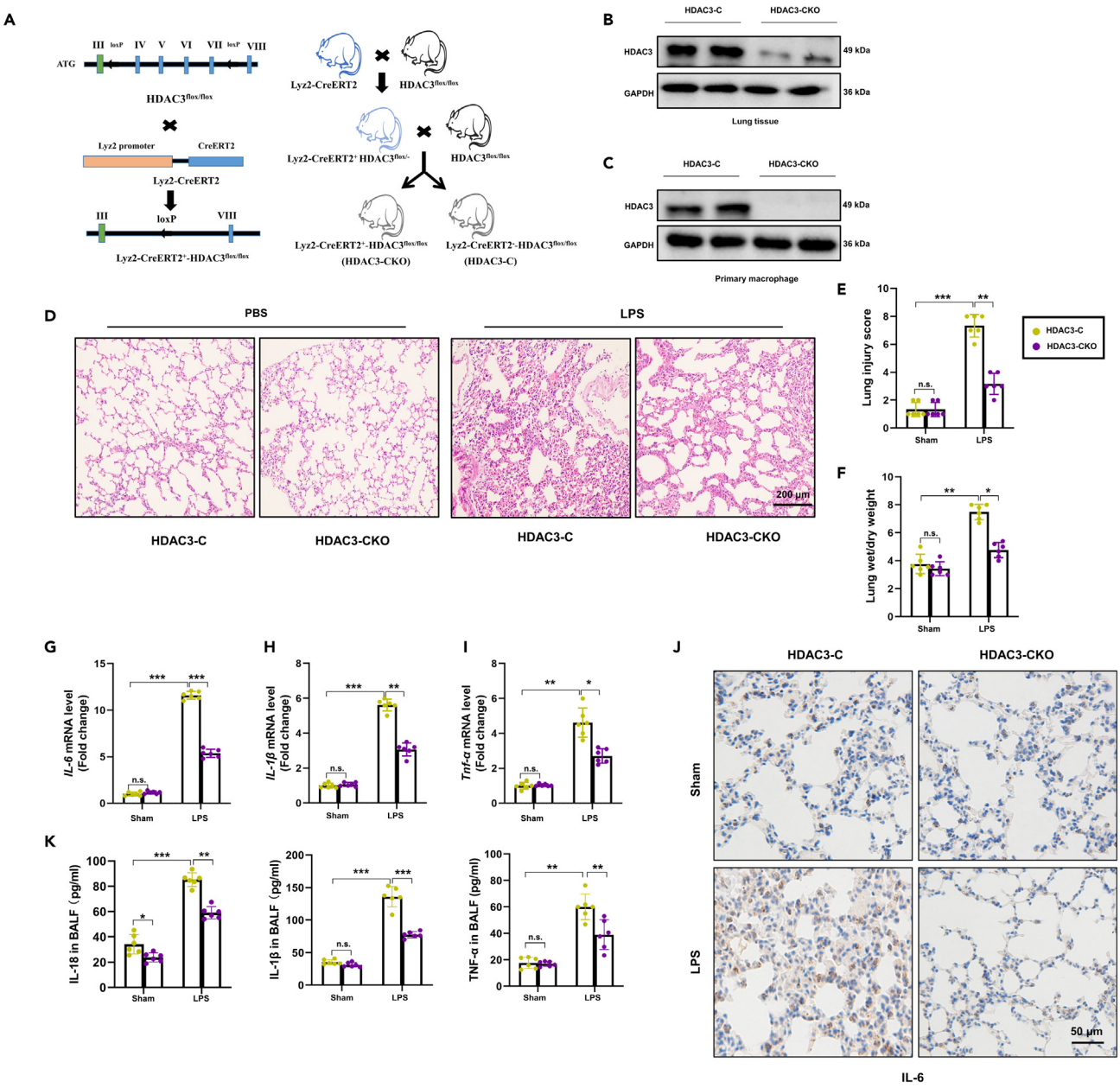

Figure 3. Comparison of the severity of lung pathological and inflammation between HDAC3-C and HDAC3-CKO mice after LPS induction

(A) HDAC3$^{flox/flox}$ mice were generated by inserting two *LoxP* sequences in the same direction into the introns flanked with the exon 4, 5, 6, and 7 of HDAC3 using CRISPR-Cas9 system, producing a nonfunctional HDAC3 protein. Lyz2-CreERT2 transgenic mice were then crossed with HDAC3$^{flox/flox}$ mice to generate the macrophage-specific HDAC3-knockout mice, named as Lyz2-CreERT2^{+}-HDAC3$^{flox/flox}$.

(B and C) Western blot analysis of HDAC3 in lung tissues and primary macrophages from HDAC3-C and HDAC3-CKO mice (n = 6).

(D and E) Histological analyses of the H&E staining and lung injury score of HDAC3-C and HDAC3-CKO mice after LPS induction (n = 6).

(F) Lung wet/dry weight (n = 6).

(G–I) Relative mRNA levels of IL-6, IL-1β, and Tnf-α in HDAC3-C and HDAC3-CKO mice after LPS induction (n = 6).

(J) Immunohistochemical staining of IL-6 in lung tissues.

(K) The protein levels of IL-18, IL-1β, and TNF-α in the obtained bronchial lavage fluid detected by ELISA (n = 6). Values represent the mean ± SEM. *p < *0.05*, **p < *0.01*, ***p < *0.001* versus the matched groups, n.s. represents no significance.

the expression of cGAS. mtDNA could be recognized by the DNA sensor cGAS in cytosol, subsequently activating STING-mediated innate immune by generating the second messenger cGAMP.[24] Hence, the level of mtDNA in cytosol was detected. The results showed that HDAC3 inhibition displayed no effects

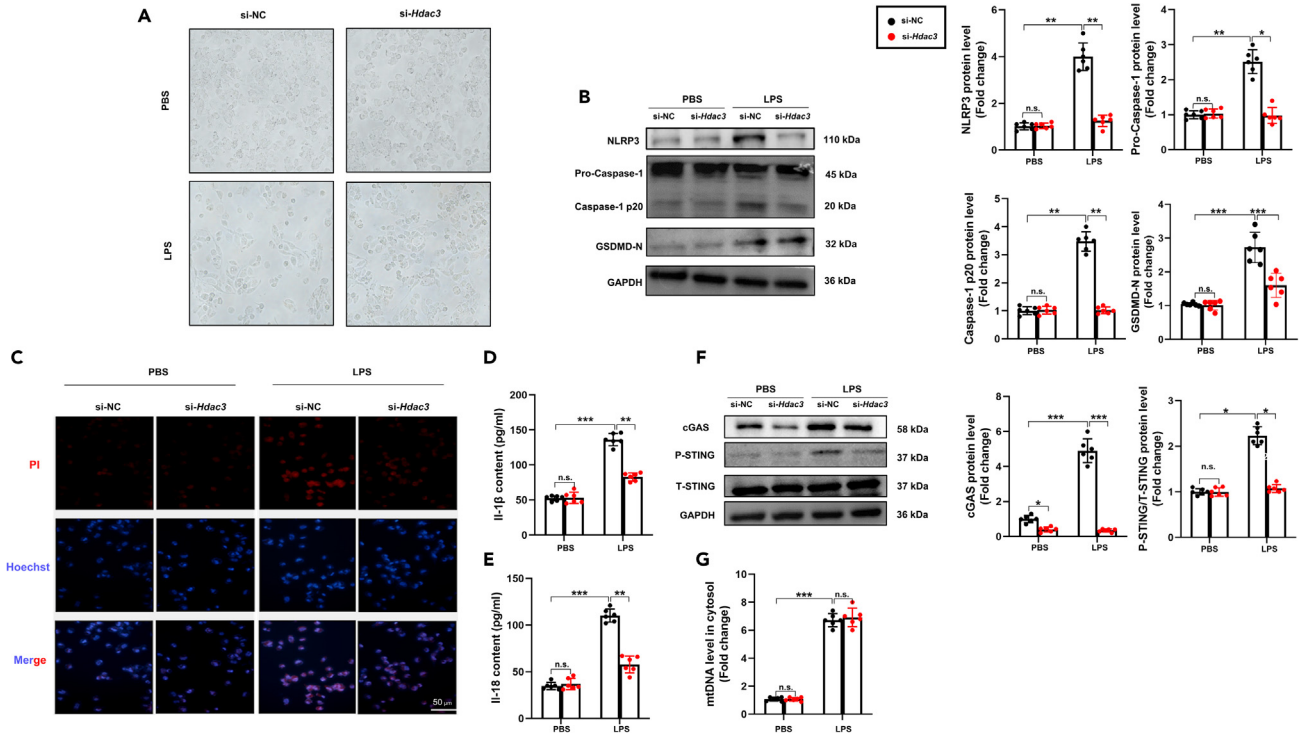

Figure 4. HDAC3 deficiency inhibited LPS-induced pyroptosis in macrophage

(A) Morphological differences of THP-1 cells observed by inverted microscopy after LPS challenge or si-*Hdac3* intervention (n = 6).

(B) Western blot analysis of NLRP3, Pro-caspase-1, Caspase-1 p20, and GSDMD-N in differentiated THP-1 cells transfected with si-*Hdac3* (n = 6).

(C) PI-Hoechst staining in differentiated THP-1 cells transfected with si-*Hdac3* (n = 6).

(D and E) IL-1β and IL-18 content in differentiated THP-1 cells (n = 6).

(F) Western blot analysis of cGAS, p-STING, and T-STING in differentiated THP-1 cells transfected with si-*Hdac3* (n = 6).

(G) Relative mtDNA level in cytosol of differentiated THP-1 cells (n = 6). Values represent the mean ± SEM. *p < *0.05*, **p < *0.01*, ***p < *0.001* versus the matched groups, n.s. represents no significance.

on the level of mtDNA in cytosol at both baseline and LPS stimulation (Figure 4G). In addition, we also detected the expression of cGAS/STING/NLRP3 pathway in HDAC3-CKO mice with ALI. The results also showed that in LPS-treated mice, HDAC3 deficiency in macrophages could inhibit the activation of cGAS/STING/NLRP3 pathway in lung tissues (Figures S3A and S3B). Similarly, at baseline, HDAC3 deficiency could downregulate the protein level of cGAS. These data further unveiled that HDAC3 may participate in the activation of cGAS/STING pathway in LPS-treated macrophage by regulating cGAS expression but not mtDNA release. Similarly, the role of HDAC3 overexpression was also explored. As shown in Figures S4A–S4C, HDAC3 overexpression further activated LPS-induced cGAS/STING pathway as well as pyroptosis in macrophage. At baseline, HDAC3 overexpression significantly increased the protein level of cGAS but showed no effects on pyroptosis, suggesting that LPS-induced mtDNA release was essential for HDAC3-mediated activation of cGAS/STING pathway and pyroptosis in macrophages.

cGAS overexpression abolished the inhibition of LPS-induced inflammation and pyroptosis by HDAC3 knockdown in macrophage

To further confirm the role of cGAS/STING pathway in the inhibition of LPS-induced pyroptosis by HDAC3 knockdown in macrophage, we next upregulated cGAS in differentiated THP-1 cells by transfecting Ad-*cGAS*. As shown in Figures 5A–5C, HDAC3 inhibition significantly decreased LPS-induced inflammatory response, evidenced by decreased mRNA levels of *Tnf-α*, *Il-6*, and *Ccl-2*. However, the mRNA levels of these pro-inflammatory genes showed no differences between the LPS+si-NC+Ad-cGAS group and the LPS+si-*Hdac3*+Ad-cGAS group. Meanwhile, we also found that cGAS overexpression also abolished the inhibition of LPS-induced pyroptosis by HDAC3 knockdown in macrophage, which was evidenced by the levels of IL-1β and IL-18 (Figures 5D and 5E). Western blot also unveiled that HDAC3 inhibition lost its regulatory effects on the protein expression of P-STING, NLRP3, and GSDMD-N in cGAS-overexpressing macrophages

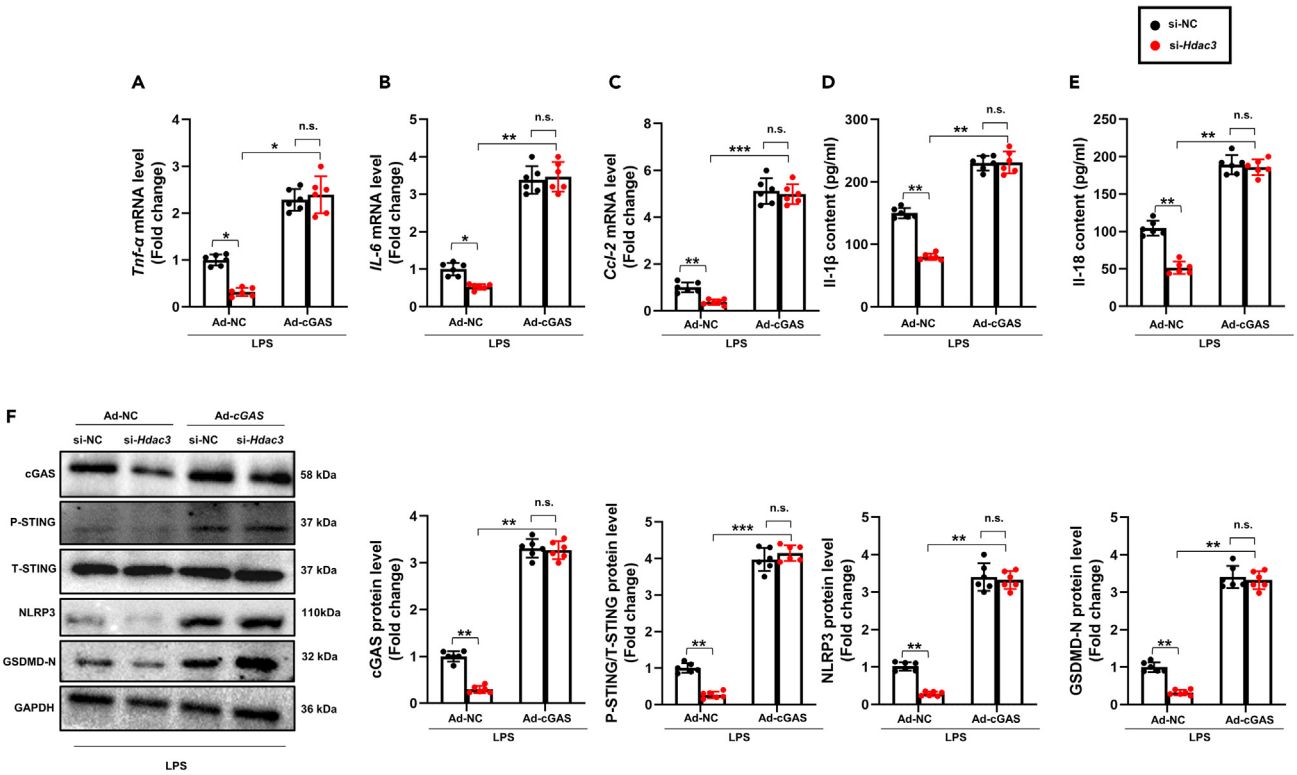

Figure 5. cGAS overexpression abolished the inhibition of LPS-induced inflammation and pyroptosis by HDAC3 knockdown in macrophage

(A–C) Relative mRNA levels of Tnf-α, IL-6, and Ccl-2 in the indicated groups (n = 6).

(D–E) IL-1β and IL-18 content in the indicated groups (n = 6).

(F) Western blot analysis of cGAS, P-STING, T-STING, NLRP3, and GSDMD-N in the indicated groups (n = 6). Values represent the mean ± SEM. *p < *0.05*, **p < *0.01*, ***p < *0.001* versus the matched groups, n.s. represents no significance.

challenged with LPS. Meanwhile, in HDAC3-knockdown macrophages challenged with LPS, cGAS overexpression significantly promoted the activation of pyroptosis (Figure 5F). Collectively, these data supported that HDAC3 deficiency could inhibit LPS-induced pyroptosis in a cGAS-dependent manner.

HDAC3 regulated cGAS level by affecting its expression rather than degradation

Considering that HDAC3 could increase the protein level of cGAS in the context of both baseline and LPS stimulation, we next explored the potential mechanisms contributing to the upregulation of cGAS by HDAC3. Firstly, the transcriptional level of cGAS was investigated. As shown in Figure 6A, HDAC3 inhibition significantly decreased the mRNA level of *cGAS* at baseline. Meanwhile, in differentiated THP-1 cells in response to LPS challenge, the mRNA level of cGAS was also suppressed by HDAC3 inhibition, hinting that HDAC3 may regulate the transcription of cGAS. Next, we also explored whether HDAC3 could affect the protein degradation of cGAS. Proteasomal activity was found to be increased in differentiated THP-1 cells in response to LPS challenge. However, HDAC3 knockdown had no effects on proteasomal activity (Figures 6B–6D). To confirm that HDAC3 was not involved in the protein degradation of cGAS, 3-MA or proteasome inhibitor MG-132 was used to block autophagy or proteasomal activity, respectively. As expected, in HDAC3-knockdown macrophages stimulated with LPS, MG-132 treatment did not affect the protein level of cGAS (Figure 6E). Not surprisingly, we concluded after intervention by the autophagy inhibitor 3-MA that HDAC3 also did not affect cGAS protein level via autophagy (Figure 6F). Taken together, these results further demonstrated that HDAC3 regulated the protein level of cGAS by affecting its mRNA transcription rather than protein degradation.

HDAC3 promoted the mRNA transcription of cGAS through inhibiting histone acetylation of miR-4767 gene promoter

It is well known that histone acetylation is usually associated with chromatin decondensation as well as gene activation.[25] Hence, HDAC3 together with other members in HDACs are supposed to repress

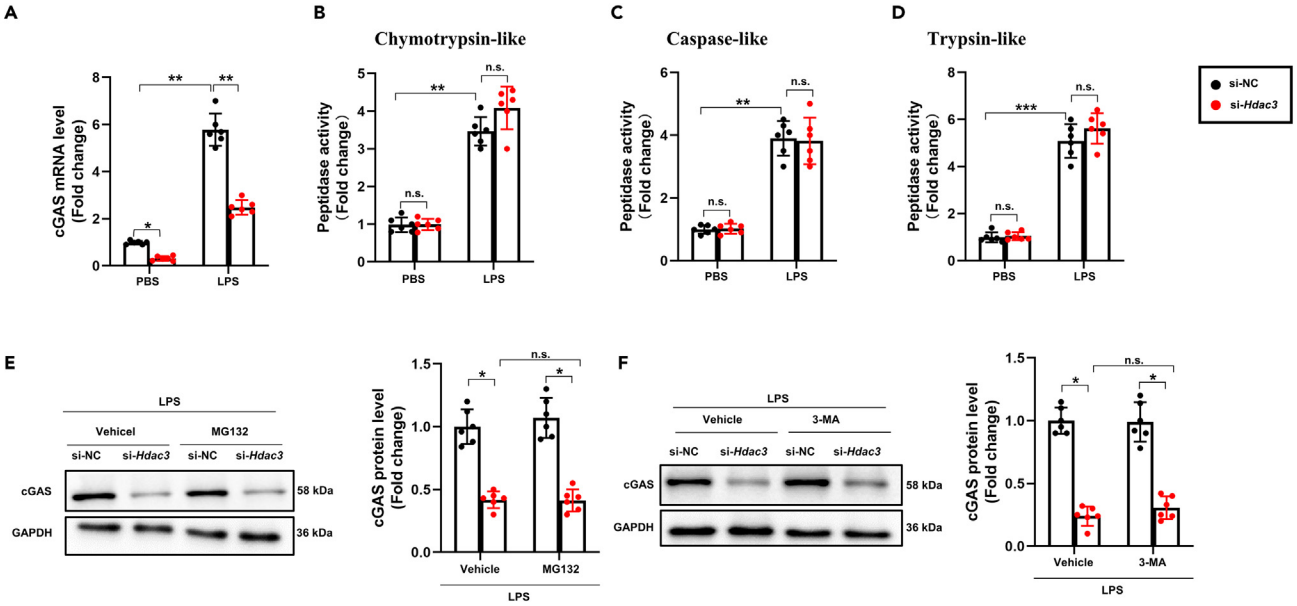

Figure 6. HDAC3 regulated cGAS level by affecting its expression rather than degradation

(A) Relative mRNA levels of cGAS in Hdac3-knockdown THP-1 cells following LPS/nigericin induction (n = 6).

(B–D) Relative proteasomal activities in Hdac3-knockdown THP-1 cells following LPS/nigericin induction (n = 6).

(E) Western blot analysis of cGAS in Hdac3-knockdown THP-1 cells following LPS/nigericin induction after proteasome inhibition (n = 6).

(F) Western blot analysis of cGAS in Hdac3-knockdown THP-1 cells following LPS/nigericin induction after autophagy inhibition (n = 6). Values represent the mean ± SEM. *p < *0.05*, **p < *0.01*, ***p < *0.001* versus the matched groups, n.s. represents no significance.

gene expression by directly regulating histone acetylation of certain genes. In view of the fact that the level of HDAC3 showed positive correlation with the expression of cGAS in this study, we thus excluded the possibility that HDAC3 could deacetylate the histones of cGAS gene promoter. Subsequently, we determined the effects of microRNA (miRNA) on the mRNA transcription of cGAS. And potential miRNAs targeting cGAS mRNA including miR-19a-3p, miR-19b-3p, miR-3121-3p, miR-548o-3p, miR-1277-5p, miR-58j-5p, and miR-4767 were screened by online tool Targetscan (http://www.targetscan.org/vert_70/) and miRTarBase (http://mirtarbase.mbc.nctu.edu.tw/php/index.php). As shown in Figure 7A, LPS significantly decreased the levels of miR-58j-5p and miR-4767, hinting that miR-58j-5p and miR-4767 may be involved in HDAC3-mediated cGAS upregulation. Furthermore, we found that HDAC3 knockdown significantly increased the levels of miR-4767 in differentiated THP-1 cells in response to LPS challenge (Figure 7B). Figure 7C showed the binding sequence of miR-4767 to the 3′UTR of cGAS mRNA by the Starbase website. The data of dual luciferase reporter assay unveiled that miR-4767 agomir reduced the luciferase activity of cGAS-WT, while showing no effects on the luciferase activity of cGAS-MUT (Figure 7D). Additionally, upon transfection with miR-4767 agomir in THP-1 cells, the expression of miR-4767 was upregulated while the protein level of cGAS was significantly downregulated (Figures 7E and 7F). By contrast, after THP-1 cells were transfected with miR-4767 antagomir, the expression of miR-4767 was significantly inhibited while the protein level of cGAS was significantly upregulated (Figures 7G and 7H). Chromatin immunoprecipitation (ChIP) assay unveiled that HDAC3 together with H3K9Ac was significantly recruited to the miR-4767 gene promoter in THP-1 cells after transduction with Ad-*Hdac3* (Figures 7I and 7J). When HDAC3 was knocked down with si-*Hdac3*, the binding between H3K9Ac and miR-4767 promoter was significantly enhanced, apart from the increased level of H3K9Ac (Figures 7K and 7L). Collectively, these data demonstrated that HDAC3 may promote cGAS expression through inhibiting histone acetylation of miR-4767 gene promoter.

miR-4767 antagomir abolished the protective roles of HDAC3 deficiency in macrophage in LPS-treated mice

To further confirm that miR-4767 was involved in HDAC3 deficiency-mediated pulmonary protection during ALI *in vivo*, miR-4767 antagomir was injected to upregulate miR-4767 level *in vivo* (Figure 8D). H&E staining and lung wet/dry weight ratio showed that miR-4767 upregulation significantly aggravated lung

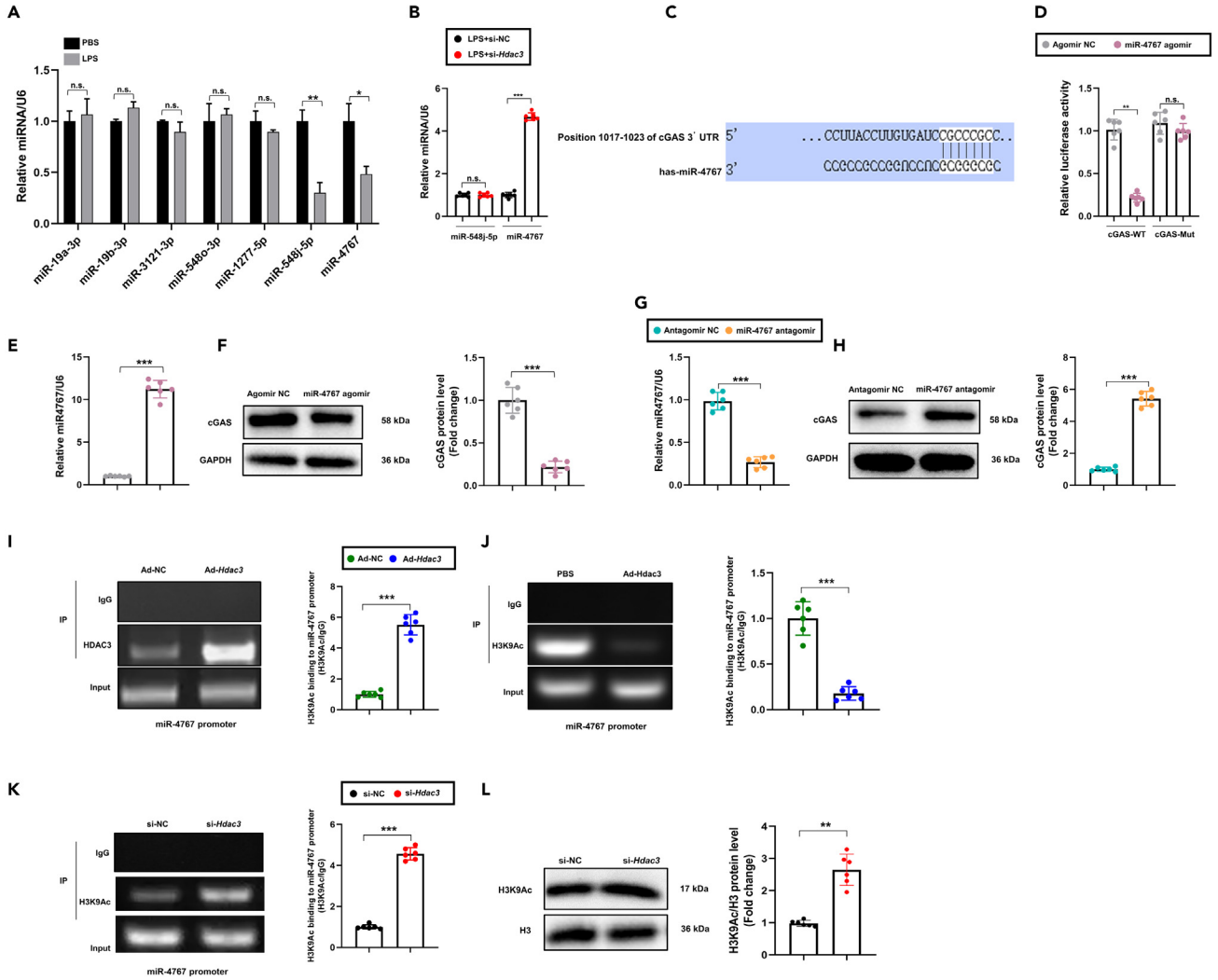

Figure 7. HDAC3 promoted the mRNA transcription of cGAS through inhibiting histone acetylation of miR-4767 gene promoter

(A) The levels of potential miRNAs targeting cGAS mRNA in differentiated THP-1 cells following LPS/nigericin induction (n = 6).

(B) The levels of miR-548j-5p and miR-4767 in Hdac3-knockdown THP-1 cells following LPS/nigericin induction (n = 6).

(C) Putative miR-4767 binding sites in the 3'UTR of cGAS mRNA.

(D) Binding of miR-4767 to cGAS verified via dual luciferase reporter gene assay in THP-1 cells (n = 6).

(E) Relative miR-4767 level in differentiated THP-1 cells stimulated with miR-4767 agomir or Agomir NC (n = 6).

(F) Western blot analysis of cGAS in differentiated THP-1 cells stimulated with miR-4767 agomir or Agomir NC (n = 6).

(G) Relative miR-4767 level in differentiated THP-1 cells stimulated with miR-4767 antagomir or Antagomir NC (n = 6).

(H) Western blot analysis of cGAS in differentiated THP-1 cells stimulated with miR-4767 antagomir or Antagomir NC (n = 6).

(I) The regulatory effect of HDAC3 on miR-4797 promoter in differentiated THP-1 cells was assessed via CHIP assay (n = 6).

(J) The regulatory effect of H3K9Ac on miR-4797 promoter in Ad-*Hdac3*-transduced THP-1 cells was assessed via CHIP assay (n = 6).

(K) The regulatory effect of H3K9Ac on miR-4797 promoter in si-*Hdac3*-transfected THP-1 cells was assessed via CHIP assay (n = 6).

(L) Western blot analysis of H3K9Ac in si-*Hdac3*-transfected THP-1 cells (n = 6). Values represent the mean ± SEM. *p < *0.05*, **p < *0.01*, ***p < *0.001* versus the matched groups, n.s. represents no significance.

pathological injury and edema in macrophage HDAC3-deficient mice injected with LPS (Figures 8A–8C). Compared with LPS+Antagomir NC group, the mRNA levels of *Tnf-α* and *Il-6* in LPS+miR-4767 antagomir group were significantly increased (Figures 8D and 8E). Finally, the proteins associated with cGAS/STING pathway and NLRP3 inflammasome were also detected. As shown in Figure 8F, the protein levels of cGAS, P-STING, NLRP3, Caspase-1 p20, and GSDMD-N in LPS+miR-4767 antagomir group were higher than those in LPS+Antagomir NC group (Figure 8G). Taken together, these *in vivo* data further demonstrated that HDAC3 deficiency prevented LPS-induced ALI in an miR-4767-dependent manner.

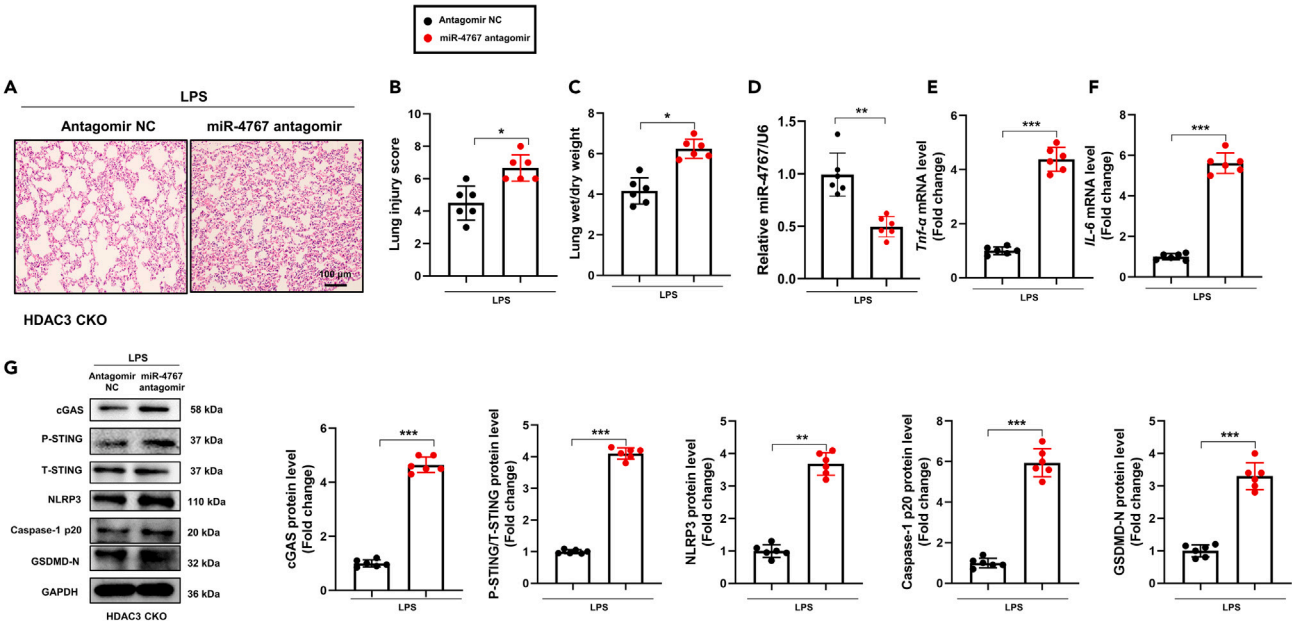

Figure 8. miR-4767 antagomir abolished the protective roles of HDAC3 deficiency in macrophage in LPS-treated mice

(A and B) Histological analyses of the H&E staining and lung injury score of LPS-treated HDAC3-CKO mice injected with antagomir NC or miR-4767 antagomir (n = 6).

(C) Lung wet/dry weight (n = 6).

(D) The level of miR-4767 in lung tissues (n = 6).

(E and F) Relative mRNA levels of Tnf-α and IL-6 in LPS-treated HDAC3-CKO mice injected with antagomir NC or miR-4767 antagomir (n = 6).

(G) Western blot analysis of cGAS, P-STING, T-STING, NLRP3, and GSDMD-N in LPS-treated HDAC3-CKO mice injected with antagomir NC or miR-4767 antagomir (n = 6). Values represent the mean ± SEM. *p < *0.05*, **p < *0.01*, ***p < *0.001* versus the matched groups, n.s. represents no significance.

Intratracheal administration of *Hdac3* siRNA-loaded liposomes prevented LPS-induced ALI in mice

Finally, we intended to translate our findings into a therapeutic strategy against ALI. Therefore, lipid-based liposomes loaded with *Hdac3* siRNA were generated via a simple and tested liposome formulation (Figure 9A). The In Vivo Imaging System (IVIS) was used to display biodistribution of liposomes by tracking the fluorescence of lipophilic carbocyanine DiOC18(7) (DiR). These liposomes administered intratracheally accumulated in the lung tissues sustainably for at least 48 h. Biodistribution of liposomes in other organs involving heart, liver, spleen, and kidney was also confirmed after intratracheal injection for 48 h. As expected, the liposomes were absent in other organs but mainly distributed in lung tissues (Figure 9B). Next, we further addressed the effect of liposomes loaded with *Hdac3* siRNA on gene expression in lung tissues. We detected the mRNA level of *Hdac3* at different time points after intratracheal administration. As shown in Figure 9C, after intratracheal administration of *Hdac3* siRNA-loaded liposomes for 36 h, an obvious decrease in *Hdac3* mRNA expression was found. The mRNA expression of *Hdac3* in *Hdac3* siRNA group was significantly lower than that in scrambled siRNA group at 48 h. To this end, wild-type mice were administrated intratracheally with *Hdac3* siRNA-loaded liposomes 36 h prior to LPS exposure. After LPS treatment for 12 h, mice were sacrificed by cervical dislocation for the assessment of lung injury (Figure 9D). We found that miR-4767 was significantly upregulated in lung tissues of mice (Figure 9J). And the results demonstrated that mice receiving *Hdac3* siRNA-loaded liposomes displayed alleviative lung pathological injury, edema, and inflammatory response after LPS stimulation (Figures 9E–9I). Not only that, western blot also showed that administration of *Hdac3* siRNA-loaded liposomes significantly inhibited the activation of cGAS/STING pathway as well as NLRP3 inflammasome (Figure 9K). In brief, these data supported that intratracheal administration of *Hdac3* siRNA-loaded liposomes may serve as a promising strategy against sepsis-induced ALI in clinical settings.

DISCUSSION

In this study, we unveiled that LPS stimulation upregulated the expression of HDAC3 and macrophage-specific deletion of HDAC3. And *Hdac3* siRNA-loaded liposomes significantly alleviated tissue damage and

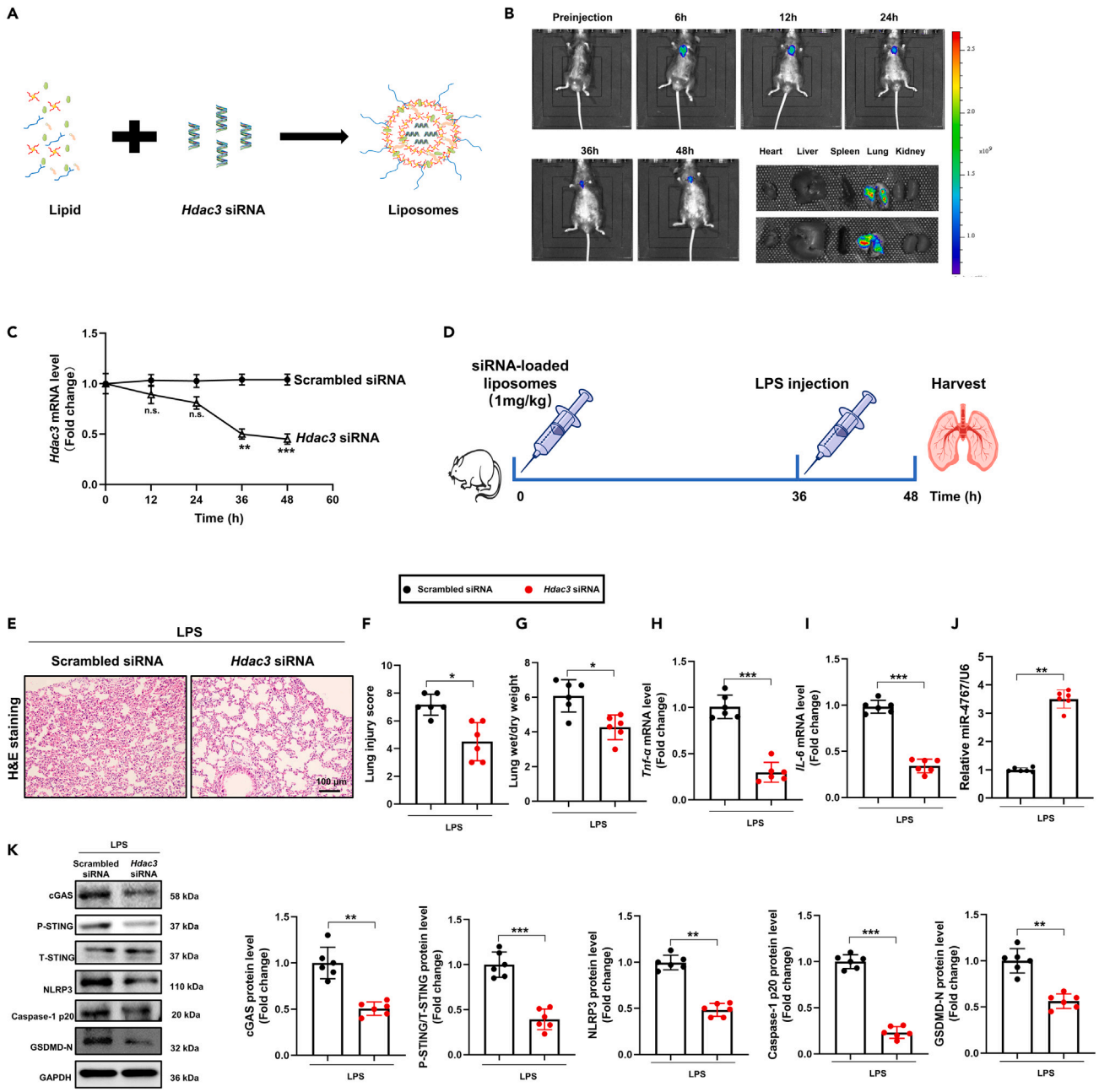

Figure 9. Intratracheal administration of *Hdac3* siRNA-loaded liposomes prevented LPS-induced ALI in mice

(A) A schematic diagram showing the preparation of *Hdac3* siRNA-loaded liposomes.

(B) Representative IVIS images of the mouse treated R-labeled liposomes as well as *ex vivo* fluorescence images of heart, liver, spleen, lung, and kidney from mice.

(C) Temporal *Hdac3* mRNA level alterations in the lung tissues from mice treated with *Hdac3* siRNA-loaded or *scrambled* siRNA-loaded liposomes (n = 6).

(D) A schematic diagram showing experimental design of LPS-treated mice administered with either *Hdac3* siRNA-loaded or *Scrambled* siRNA-loaded liposomes (n = 6).

(E and F) Histological analyses of the H&E staining and lung injury score of LPS-treated WT mice administered with either *Hdac3* siRNA-loaded or *Scrambled* siRNA-loaded liposomes. (n = 6).

(G) Lung wet/dry weight (n = 6).

(H and I) Relative mRNA levels of Tnf-α and IL-6 in LPS-treated WT mice administered with either *Hdac3* siRNA-loaded or *Scrambled* siRNA-loaded liposomes. (n = 6).

(J) The level of miR-4767 in lung tissues (n = 6).

Figure 9. *Continued*

(K) Western blot analysis of cGAS, P-STING, T-STING, NLRP3, and GSDMD-N in LPS-treated mice administered with either *Hdac3* siRNA-loaded or *Scrambled* siRNA-loaded liposomes (n = 6). Values represent the mean ± SEM. *p < *0.05*, **p < *0.01*, ***p < *0.001* versus the matched groups, n.s. represents no significance.

pyroptosis in LPS-induced ALI in mice. In keeping with the *in vivo* data, HDAC3 inhibition by siRNA exerted similar protective effects on LPS-induced inflammatory response and pyroptosis in macrophage. In terms of mechanism, we identified that HDAC3 could activate cGAS/STING pathway through decreasing histone acetylation of the miR-4767 gene promoter in LPS-induced macrophage, thus triggering inflammation and pyroptosis. Based on these data, we supposed that HDAC3 was a potential therapeutic target for the prevention of LPS-induced ALI.

Epigenetic modifications could modulate gene expression as well as developmental programs without changing the gene sequence.[26] As one of the critical manners of epigenetic modifications, histone modification involving acetylation and deacetylation is related with various pathological and physiological processes in mammal. Under different pathological status, epigenetically modified histones in eukaryotic cells could modulate gene expression by stabilizing chromatin structure, triggering oxidative stress, inflammation, as well as cell death.[14] As one of the members in HDAC, HDAC3, has been reported to participate in various inflammatory conditions, organ fibrosis, neurodegeneration, and ischemic injury by mediating histone deacetylation through promoting chromatin condensation as well as transcriptional repression.[27] Wang Di et al.[28] found that HDAC3 was significantly upregulated in lung tissues from mice with bronchopulmonary dysplasia. Another study showed that HDAC3 deficiency in early embryonic development gave rise to abnormal development of alveolar macrophages, while HDAC3 deficiency after birth resulted in abnormal homeostasis and maturation in alveolar macrophages.[29] These studies suggested that HDAC3 was essential for normal pulmonary development in mammals. In addition, during cold storage/transplantation-induced acute kidney injury, HDAC3 inhibition by RGFP966 reduced the mitochondrial pathway of apoptosis and maintained mitochondrial membrane potential in proximal tubular cell.[21] Macrophage-specific deletion of HDAC3 shared a similar polarized behavior with IL-4-induced alternative activation, thus blocking the progress of atherosclerosis.[30] Gioacchino Natoli et al. also reported that LPS stimulation failed to activate the expression of nearly half of the inflammatory genes in macrophage when HDAC3 was repressed, hinting that HDAC3 silencing displayed anti-inflammatory potential.[31] One recent study also showed that catalytic activity as well as its enzymatic activity may play dichotomous roles during inflammatory responses.[22] However, there is no available data about the roles of HDAC3 in LPS-induced ALI. Here, we observed that HDAC3 deficiency in macrophages significantly relieved LPS-elicited inflammation and pyroptosis. Macrophage-specific deletion of HDAC3 or *Hdac3* siRNA-loaded liposomes obviously prevented lung pathological injury and inflammation in LPS-treated mice. Overactivated inflammatory response and excessive infiltration of macrophages in lung tissue are vital pathological features during LPS-induced ALI.[32] In the present study, we found that the level of HDAC3 was correlated with the intensity of macrophages in lung tissues, which hinted that HDAC3 in macrophage was implicated with inflammation and ALI. Additionally, we also found that HDAC3 deficiency or overexpression at baseline displayed no effects on inflammation and pyroptosis, suggesting that LPS stimulation was essential for the effects of HDAC3. Unfortunately, the mechanism by which HDAC3, a key factor in the regulation of immune responses, is regulated *in vivo* remains heavily questioned. Recent studies have reported that nicotinamide adenine dinucleotide phosphate (NADPH) , a substrate for lipid biosynthesis, can activate HDAC3 and upregulate its expression.[33] The accumulation of NADPH after LPS stimulation is likely to be one of the important reasons for the elevated HDAC3 expression; however, this still needs a lot of experiments to prove.

cGAS/STING pathway is an important DNA sensing signal, which could evoke the generation of type I interferon by activating nuclear factor κB (NF-κB) and interferons regulatory factor 3 (IRF3). A great many studies have demonstrated that the hyperactivation of cGAS/STING pathway gives rise to cellular senescence,[34,35] autoimmunity,[36] infection,[37] and regulated cell death.[11,38] In macrophages, the activation of cGAS/STING pathway could promote them to polarize into M1 phenotype.[39] In addition, STING could interact with NLRP3 and reduce K48- and K63-linked polyubiquitination of NLRP3, thus resulting in the inflammasome activation.[40] In our previous studies, we found that the activation of STING/IRF3 pathway by LPS triggered pyroptosis in cardiomyocytes, thus aggravating sepsis-induced cardiac dysfunction and injury.[38] In LPS-induced macrophages, TLR4-mediated release of mtDNA into cytoplasm further activated cGAS-STING-NLRP3 axis, eventually giving rise to pyroptosis and pathological injury in murine lung tissues.[11] mtDNA

also triggered autophagy dysfunction in macrophage through activating cGAS/STING pathway, which served as another critical mechanism contributing to ALI.[41] Here, we observed that HDAC3 silencing significantly inhibited LPS-induced activation of cGAS/STING pathway as well as pyroptosis in macrophages *in vivo* and *in vitro*. At baseline, HDAC3 silencing could decrease the protein and mRNA levels of cGAS while it showed no effects on the phosphorylation of STING. Similarly, HDAC3 overexpression at baseline upregulated the expression of cGAS without affecting the activation of STING and NLRP3 inflammasome. We also found that HDAC3 silencing did not affect mtDNA level in cytoplasm regardless of LPS stimulation. From our perspective, mtDNA release triggered by LPS was essential HDAC3-mediated pyroptosis in macrophages and ALI. At baseline, HDAC3-mediated upregulation of cGAS is insufficient to activate STING and NLRP3 inflammasome for the reason that cGAS was not activated by mtDNA in cytoplasm. Meanwhile, we also investigated how HDAC3 regulated the level of cGAS in macrophages. We found that HDAC3 silencing did not affect autophagy and proteasomal activity in LPS-induced macrophages while HDAC3 silencing significantly upregulated the mRNA level of cGAS. Therefore, we dare to speculate that HDAC3-mediated protein upregulation of cGAS was involved in transcriptional activation of *cgas* gene.

miRNA serves as a type of small noncoding RNA, playing a crucial role in ALI/ARDS by regulating immune response and inflammatory response through chiefly binding to the 3′-UTR of mRNA to suppress or degrade the expression of target genes.[42] As we mentioned earlier, histone acetylation usually gives rise to chromatin decondensation and gene activation. Hence, HDAC3 is not supposed to repress expression of cGAS gene by directly regulating its histone acetylation. Therefore, we mainly focused on the effects of miRNA on the mRNA transcription of cGAS gene. And we found that cGAS acted as a direct target gene of miR-4767 in macrophage. LPS could recruit HDAC3 and H3K9Ac to the miR-4767 gene promoter, repressing the expression of miR-4767 by decreasing histone acetylation of gene promoter.

The nanodrug delivery system containing nuclear acid displays multiple advantages in disease treatment, including high encapsulation efficiency, excellent biocompatibility, enhanced targeting capability, as well as reduced gene degradation.[43] As a novel nanodrug delivery system, liposomes could finely control drug release after they are inhaled into the lung tissues. In addition, liposomes can be efficiently internalized and phagocytosed by macrophages in lung tissues.[44] Here, we observed that intratracheal administration of *Hdac3* siRNA-loaded liposomes significantly alleviated LPS-induced lung pathological injury and blocked the activation of cGAS/STING pathway, indicating that it was possible using *Hdac3* siRNA-loaded liposomes as an alternative strategy for the therapy of LPS-induced ALI.

In conclusion, our study showed that HDAC3 played a pivotal role in mediating pyroptosis in macrophage by activating cGAS/STING pathway through decreasing histone acetylation of the miR-4767 gene promoter, thereby exacerbating the inflammatory response of LPS-induced ALI. We innovatively encapsulated *Hdac3* siRNA into liposomes and targeted it to lung macrophages, providing a new idea for clinical translation while demonstrating that HDAC3 is a key pro-inflammatory molecule in ALI. Although our study still has the limitation of failing to confirm the optimal dose as well as the timing of the therapeutic effect of Hdac3 siRNA-loaded liposomes, this does not detract from our conclusion that targeting HDAC3 in macrophage may provide a new therapeutic target for the prevention of LPS-induced ALI.

Limitations of the study

The study mainly explored the role of HDAC3 in activating the cGAS/STING pathway through histone deacetylation in macrophages to promote pyroptosis and aggravate LPS-induced ALI. *In vivo* experiments, we observed that HDAC3 was also abnormally expressed in alveolar epithelial cells, and the specific mechanism will be verified in future studies. In consideration of the experimental conditions and equipment requirements, we have not verified the existence time of siRNA-loaded liposomes *in vivo*, the degree of phagocytosis by macrophages in lung tissue, and the optimal concentration of action. The possible errors in this study come from the random nature of the samples and experimental animals on the one hand and the subjective errors of the experimental personnel on the other hand.

STAR★METHODS

Detailed methods are provided in the online version of this paper and include the following:

- KEY RESOURCES TABLE
- RESOURCE AVAILABILITY

- Lead contact
- Materials availability
- Data and code availability
- EXPERIMENTAL MODEL AND SUBJECT DETAILS
  - Animals and treatment
  - Cell culture and treatment
- METHOD DETAILS
  - Histopathological analysis
  - Real-time PCR and western blot
  - PI-Hoechst staining
  - The determination of HMGB1, IL-1β, IL-18 and TNF-α
  - Cell viability
  - The detection of mitochondrial DNA in cytoplasm
  - Proteasomal activity
  - Dual-luciferase reporter gene assay
  - Chromatin immunoprecipitation (CHIP)
  - Preparation and characterization of *Hdac3* siRNA-loaded liposomes
  - Statistical analysis

SUPPLEMENTAL INFORMATION

Supplemental information can be found online at https://doi.org/10.1016/j.isci.2023.107158.

ACKNOWLEDGMENTS

We thanked for the support of grants from the National Natural Science Foundation of China, the Fundamental Research Funds for the Central Universities, and Science Fund for Creative Research Groups of the Natural Science Foundation of Hubei Province. Meanwhile, we thanked for the platform support from Wuhan University.

Sources of funding: This work was supported by grants from the National Natural Science Foundation of China (No. 8210082163, 81770095, 81800343), the Fundamental Research Funds for the Central Universities (No. 2042021kf0081), and Science Fund for Creative Research Groups of the Natural Science Foundation of Hubei Province (No. 2020CFA027).

Declarations: Ethics approval Animal experiments were approved by the Animal Ethics Committee of Renmin Hospital, Wuhan University (Approval Number: WDRM20210305) and strictly performed according to the Guide for the Care and Use of Laboratory Animals published by the US National Institutes of Health.

AUTHOR CONTRIBUTIONS

Li Ning, Liu Bohao, Xiong Rui, Wang Bo, and Geng Qing contributed to conception, designed experiments, and were responsible for the whole work; Liu Bohao, Xiong Rui, He Ruyuan, Li Guorui, Fu Tinglv, and Xu Chenzhen performed experiments; Li Ning and Liu Bohao analyzed experimental results and wrote the manuscript.

DECLARATION OF INTERESTS

The authors declare no competing interests.

INCLUSION AND DIVERSITY

We support inclusive, diverse, and equitable conduct of research.

Received: March 2, 2023
Revised: April 14, 2023
Accepted: June 12, 2023
Published: June 19, 2023

REFERENCES

1. Qian, Y., Wang, Z., Lin, H., Lei, T., Zhou, Z., Huang, W., Wu, X., Zuo, L., Wu, J., Liu, Y., et al. (2022). TRIM47 is a novel endothelial activation factor that aggravates lipopolysaccharide-induced acute lung injury in mice via K63-linked ubiquitination of TRAF2. Signal Transduct. Targeted Ther. *7*, 148. https://doi.org/10.1038/s41392-022-00953-9.

2. Butt, Y., Kurdowska, A., and Allen, T.C. (2016). Acute Lung Injury: A Clinical and Molecular Review. Arch. Pathol. Lab Med. *140*, 345–350. https://doi.org/10.5858/arpa.2015-0519-RA.

3. Mokrá, D. (2020). Acute lung injury - from pathophysiology to treatment. Physiol. Res. *69*. S353-s366. https://doi.org/10.33549/physiolres.934602.

4. Chen, X., Tang, J., Shuai, W., Meng, J., Feng, J., and Han, Z. (2020). Macrophage polarization and its role in the pathogenesis of acute lung injury/acute respiratory distress syndrome. Inflamm. Res. *69*, 883–895. https://doi.org/10.1007/s00011-020-01378-2.

5. Kopf, M., Schneider, C., and Nobs, S.P. (2015). The development and function of lung-resident macrophages and dendritic cells. Nat. Immunol. *16*, 36–44. https://doi.org/10.1038/ni.3052.

6. Byrne, A.J., Mathie, S.A., Gregory, L.G., and Lloyd, C.M. (2015). Pulmonary macrophages: key players in the innate defence of the airways. Thorax *70*, 1189–1196. https://doi.org/10.1136/thoraxjnl-2015-207020.

7. Puttur, F., Gregory, L.G., and Lloyd, C.M. (2019). Airway macrophages as the guardians of tissue repair in the lung. Immunol. Cell Biol. *97*, 246–257. https://doi.org/10.1111/imcb.12235.

8. Hsu, C.G., Chávez, C.L., Zhang, C., Sowden, M., Yan, C., and Berk, B.C. (2022). The lipid peroxidation product 4-hydroxynonenal inhibits NLRP3 inflammasome activation and macrophage pyroptosis. Cell Death Differ. *29*, 1790–1803. https://doi.org/10.1038/s41418-022-00966-5.

9. Huang, Y., Xu, W., and Zhou, R. (2021). NLRP3 inflammasome activation and cell death. Cell. Mol. Immunol. *18*, 2114–2127. https://doi.org/10.1038/s41423-021-00740-6.

10. Luo, D., Dai, W., Feng, X., Ding, C., Shao, Q., Xiao, R., Zhao, N., Peng, W., Yang, Y., Cui, Y., et al. (2021). Suppression of lncRNA NLRP3 inhibits NLRP3-triggered inflammatory responses in early acute lung injury. Cell Death Dis. *12*, 898. https://doi.org/10.1038/s41419-021-04180-y.

11. Ning, L., Wei, W., Wenyang, J., Rui, X., and Qing, G. (2020). Cytosolic DNA-STING-NLRP3 axis is involved in murine acute lung injury induced by lipopolysaccharide. Clin. Transl. Med. *10*, e228. https://doi.org/10.1002/ctm2.228.

12. Liu, B., Wang, Z., He, R., Xiong, R., Li, G., Zhang, L., Fu, T., Li, C., Li, N., and Geng, Q. (2022). Buformin alleviates sepsis-induced acute lung injury via inhibiting NLRP3-mediated pyroptosis through an AMPK-dependent pathway. Clin. Sci. (Lond.) *136*, 273–289. https://doi.org/10.1042/cs20211156.

13. Li, N., Xiong, R., He, R., Liu, B., Wang, B., and Geng, Q. (2021). Mangiferin Mitigates Lipopolysaccharide-Induced Lung Injury by Inhibiting NLRP3 Inflammasome Activation. J. Inflamm. Res. *14*, 2289–2300. https://doi.org/10.2147/JIR.S304492.

14. Park, J., Lee, K., Kim, K., and Yi, S.J. (2022). The role of histone modifications: from neurodevelopment to neurodiseases. Signal Transduct. Targeted Ther. *7*, 217. https://doi.org/10.1038/s41392-022-01078-9.

15. Susetyo, A., Ishii, S., Fujiwara, Y., Amano, I., and Koibuchi, N. (2022). Histone Deacetylase 3 Inhibitor Alleviates Cerebellar Defects in Perinatal Hypothyroid Mice by Stimulating Histone Acetylation and Transcription at Thyroid Hormone-Responsive Gene Loci. Int. J. Mol. Sci. *23*, 7869. https://doi.org/10.3390/ijms23147869.

16. Guo, Q., Kang, H., Wang, J., Dong, Y., Peng, R., Zhao, H., Wu, W., Guan, H., and Li, F. (2021). Inhibition of ACLY Leads to Suppression of Osteoclast Differentiation and Function Via Regulation of Histone Acetylation. J. Bone Miner. Res. *36*, 2065–2080. https://doi.org/10.1002/jbmr.4399.

17. Chen, T.-F., Hao, H.-F., Zhang, Y., Chen, X.-Y., Zhao, H.-S., Yang, R., Li, P., Qiu, L.-X., Sang, Y.-H., Xu, C., and Liu, S.-X. (2022). HBO1 induces histone acetylation and is important for non-small cell lung cancer cell growth. Int. J. Biol. Sci. *18*, 3313–3323. https://doi.org/10.7150/ijbs.72526.

18. Liu, G., Chen, H., Liu, H., Zhang, W., and Zhou, J. (2021). Emerging roles of SIRT6 in human diseases and its modulators. Med. Res. Rev. *41*, 1089–1137. https://doi.org/10.1002/med.21753.

19. Chen, X., He, Y., Fu, W., Sahebkar, A., Tan, Y., Xu, S., and Li, H. (2020). Histone Deacetylases (HDACs) and Atherosclerosis: A Mechanistic and Pharmacological Review. Front. Cell Dev. Biol. *8*, 581015. https://doi.org/10.3389/fcell.2020.581015.

20. Kasotakis, G., Kintsurashvili, E., Galvan, M.D., Graham, C., Purves, J.T., Agarwal, S., Corcoran, D.L., Sullenger, B.A., Palmer, S.M., and Remick, D.G. (2020). Histone Deacetylase 7 Inhibition in a Murine Model of Gram-Negative Pneumonia-Induced Acute Lung Injury. Shock *53*, 344–351. https://doi.org/10.1097/shk.0000000000001372.

21. Xiang, X., Dong, G., Zhu, J., Zhang, G., and Dong, Z. (2022). Inhibition of HDAC3 protects against kidney cold storage/transplantation injury and allograft dysfunction. Clin. Sci. (Lond.) *136*, 45–60. https://doi.org/10.1042/cs20210823.

22. Nguyen, H.C.B., Adlanmerini, M., Hauck, A.K., and Lazar, M.A. (2020). Dichotomous engagement of HDAC3 activity governs inflammatory responses. Nature *584*, 286–290. https://doi.org/10.1038/s41586-020-2576-2.

23. Zhang, F., Qi, L., Feng, Q., Zhang, B., Li, X., Liu, C., Li, W., Liu, Q., Yang, D., Yin, Y., et al. (2021). HIPK2 phosphorylates HDAC3 for NF-κB acetylation to ameliorate colitis-associated colorectal carcinoma and sepsis. Proc. Natl. Acad. Sci. USA *118*, e2021798118. https://doi.org/10.1073/pnas.2021798118.

24. Oduro, P.K., Zheng, X., Wei, J., Yang, Y., Wang, Y., Zhang, H., Liu, E., Gao, X., Du, M., and Wang, Q. (2022). The cGAS-STING signaling in cardiovascular and metabolic diseases: Future novel target option for pharmacotherapy. Acta Pharm. Sin. B *12*, 50–75. https://doi.org/10.1016/j.apsb.2021.05.011.

25. Chelladurai, P., Boucherat, O., Stenmark, K., Kracht, M., Seeger, W., Bauer, U.M., Bonnet, S., and Pullamsetti, S.S. (2021). Targeting histone acetylation in pulmonary hypertension and right ventricular hypertrophy. Br. J. Pharmacol. *178*, 54–71. https://doi.org/10.1111/bph.14932.

26. Du, W., Shi, G., Shan, C.M., Li, Z., Zhu, B., Jia, S., Li, Q., and Zhang, Z. (2022). Mechanisms of chromatin-based epigenetic inheritance. Sci. China Life Sci. *65*, 2162–2190. https://doi.org/10.1007/s11427-022-2120-1.

27. Ning, L., Rui, X., Bo, W., and Qing, G. (2021). The critical roles of histone deacetylase 3 in the pathogenesis of solid organ injury. Cell Death Dis. *12*, 734. https://doi.org/10.1038/s41419-021-04019-6.

28. Wang, D., Hong, H., Li, X.X., Li, J., and Zhang, Z.Q. (2020). Involvement of Hdac3-mediated inhibition of microRNA cluster 17-92 in bronchopulmonary dysplasia development. Mol. Med. *26*, 99. https://doi.org/10.1186/s10020-020-00237-4.

29. Yao, Y., Liu, Q., Adrianto, I., Wu, X., Glassbrook, J., Khalasawi, N., Yin, C., Yi, Q., Dong, Z., Geissmann, F., et al. (2020). Histone deacetylase 3 controls lung alveolar macrophage development and homeostasis. Nat. Commun. *11*, 3822. https://doi.org/10.1038/s41467-020-17630-6.

30. Hoeksema, M.A., Gijbels, M.J., Van den Bossche, J., van der Velden, S., Sijm, A., Neele, A.E., Seijkens, T., Stöger, J.L., Meiler, S., Boshuizen, M.C., et al. (2014). Targeting macrophage Histone deacetylase 3 stabilizes atherosclerotic lesions. EMBO Mol. Med. *6*, 1124–1132. https://doi.org/10.15252/emmm.201404170.

31. Chen, X., Barozzi, I., Termanini, A., Prosperini, E., Recchiuti, A., Dalli, J., Mietton, F., Matteoli, G., Hiebert, S., and Natoli, G. (2012). Requirement for the histone deacetylase Hdac3 for the inflammatory gene expression program in macrophages. Proc. Natl. Acad. Sci. USA *109*, E2865–E2874. https://doi.org/10.1073/pnas.1121131109.

32. Lee, J.W., Chun, W., Lee, H.J., Min, J.H., Kim, S.M., Seo, J.Y., Ahn, K.S., and Oh, S.R. (2021). The Role of Macrophages in the Development of Acute and Chronic

Inflammatory Lung Diseases. Cells *10*. https://doi.org/10.3390/cells10040897.

33. Li, W., Kou, J., Qin, J., Li, L., Zhang, Z., Pan, Y., Xue, Y., and Du, W. (2021). NADPH levels affect cellular epigenetic state by inhibiting HDAC3-Ncor complex. Nat. Metab. *3*, 75–89. https://doi.org/10.1038/s42255-020-00330-2.

34. Sladitschek-Martens, H.L., Guarnieri, A., Brumana, G., Zanconato, F., Battilana, G., Xiccato, R.L., Panciera, T., Forcato, M., Bicciato, S., Guzzardo, V., et al. (2022). YAP/TAZ activity in stromal cells prevents ageing by controlling cGAS-STING. Nature *607*, 790–798. https://doi.org/10.1038/s41586-022-04924-6.

35. Hou, Y., Wei, Y., Lautrup, S., Yang, B., Wang, Y., Cordonnier, S., Mattson, M.P., Croteau, D.L., and Bohr, V.A. (2021). NAD(+) supplementation reduces neuroinflammation and cell senescence in a transgenic mouse model of Alzheimer's disease via cGAS-STING. Proc. Natl. Acad. Sci. USA *118*, e2011226118. https://doi.org/10.1073/pnas.2011226118.

36. Wobma, H., Shin, D.S., Chou, J., and Dedeoğlu, F. (2022). Dysregulation of the cGAS-STING Pathway in Monogenic Autoinflammation and Lupus. Front. Immunol. *13*, 905109. https://doi.org/10.3389/fimmu.2022.905109.

37. Du, Y., Luo, Y., Hu, Z., Lu, J., Liu, X., Xing, C., Wu, J., Duan, T., Chu, J., Wang, H.Y., et al. (2022). Activation of cGAS-STING by Lethal Malaria N67C Dictates Immunity and Mortality through Induction of CD11b(+) Ly6C(hi) Proinflammatory Monocytes. Adv. Sci. *9*, e2103701. https://doi.org/10.1002/advs.202103701.

38. Li, N., Zhou, H., Wu, H., Wu, Q., Duan, M., Deng, W., and Tang, Q. (2019). STING-IRF3 contributes to lipopolysaccharide-induced cardiac dysfunction, inflammation, apoptosis and pyroptosis by activating NLRP3. Redox Biol. *24*, 101215. https://doi.org/10.1016/j.redox.2019.101215.

39. Ou, L., Zhang, A., Cheng, Y., and Chen, Y. (2021). The cGAS-STING Pathway: A Promising Immunotherapy Target. Front. Immunol. *12*, 795048. https://doi.org/10.3389/fimmu.2021.795048.

40. Wang, W., Hu, D., Wu, C., Feng, Y., Li, A., Liu, W., Wang, Y., Chen, K., Tian, M., Xiao, F., et al. (2020). STING promotes NLRP3 localization in ER and facilitates NLRP3 deubiquitination to activate the inflammasome upon HSV-1 infection. PLoS Pathog. *16*, e1008335. https://doi.org/10.1371/journal.ppat.1008335.

41. Liu, Q., Wu, J., Zhang, X., Li, X., Wu, X., Zhao, Y., and Ren, J. (2021). Circulating mitochondrial DNA-triggered autophagy dysfunction via STING underlies sepsis-related acute lung injury. Cell Death Dis. *12*, 673. https://doi.org/10.1038/s41419-021-03961-9.

42. Lu, Q., Yu, S., Meng, X., Shi, M., Huang, S., Li, J., Zhang, J., Liang, Y., Ji, M., Zhao, Y., and Fan, H. (2022). MicroRNAs: Important Regulatory Molecules in Acute Lung Injury/Acute Respiratory Distress Syndrome. Int. J. Mol. Sci. *23*, 5545. https://doi.org/10.3390/ijms23105545.

43. Mashel, T.V., Tarakanchikova, Y.V., Muslimov, A.R., Zyuzin, M.V., Timin, A.S., Lepik, K.V., and Fehse, B. (2020). Overcoming the delivery problem for therapeutic genome editing: Current status and perspective of non-viral methods. Biomaterials *258*, 120282. https://doi.org/10.1016/j.biomaterials.2020.120282.

44. Pan, T., Zhou, Q., Miao, K., Zhang, L., Wu, G., Yu, J., Xu, Y., Xiong, W., Li, Y., and Wang, Y. (2021). Suppressing Sart1 to modulate macrophage polarization by siRNA-loaded liposomes: a promising therapeutic strategy for pulmonary fibrosis. Theranostics *11*, 1192–1206. https://doi.org/10.7150/thno.48152.

45. Li, N., Wang, W., Zhou, H., Wu, Q., Duan, M., Liu, C., Wu, H., Deng, W., Shen, D., and Tang, Q. (2020). Ferritinophagy-mediated ferroptosis is involved in sepsis-induced cardiac injury. Free Radic. Biol. Med. *160*, 303–318. https://doi.org/10.1016/j.freeradbiomed.2020.08.009.

46. Qin, X., Zhou, Y., Jia, C., Chao, Z., Qin, H., Liang, J., Liu, X., Liu, Z., Sun, T., Yuan, Y., and Zhang, H. (2022). Caspase-1-mediated extracellular vesicles derived from pyroptotic alveolar macrophages promote inflammation in acute lung injury. Int. J. Biol. Sci. *18*, 1521–1538. https://doi.org/10.7150/ijbs.66477.

47. Chen, Y.F., Hu, F., Wang, X.G., Tang, Z., Tang, H.X., and Xu, M. (2021). MicroRNA-23a-5p Is Involved in the Regulation of Lipopolysaccharide-Induced Acute Lung Injury by Targeting HSP20/ASK1. Oxid. Med. Cell. Longev. *2021*, 9942557. https://doi.org/10.1155/2021/9942557.

48. Tong, Z., Jiang, B., Zhang, L., Liu, Y., Gao, M., Jiang, Y., Li, Y., Lu, Q., Yao, Y., and Xiao, X. (2014). HSF-1 is involved in attenuating the release of inflammatory cytokines induced by LPS through regulating autophagy. Shock *41*, 449–453. https://doi.org/10.1097/SHK.0000000000000118.

49. Hou, L., Zhang, J., Liu, Y., Fang, H., Liao, L., Wang, Z., Yuan, J., Wang, X., Sun, J., Tang, B., et al. (2021). MitoQ alleviates LPS-mediated acute lung injury through regulating Nrf2/Drp1 pathway. Free Radic. Biol. Med. *165*, 219–228. https://doi.org/10.1016/j.freeradbiomed.2021.01.045.

50. Pfaffl, M.W. (2001). A new mathematical model for relative quantification in real-time RT-PCR. Nucleic Acids Res. *29*, e45.

51. He, R., Liu, B., Xiong, R., Geng, B., Meng, H., Lin, W., Hao, B., Zhang, L., Wang, W., Jiang, W., et al. (2022). Itaconate inhibits ferroptosis of macrophage via Nrf2 pathways against sepsis-induced acute lung injury. Cell Death Dis. *8*, 43. https://doi.org/10.1038/s41420-021-00807-3.

52. Soni, S., Wilson, M.R., O'Dea, K.P., Yoshida, M., Katbeh, U., Woods, S.J., and Takata, M. (2016). Alveolar macrophage-derived microvesicles mediate acute lung injury. Thorax *71*, 1020–1029. https://doi.org/10.1136/thoraxjnl-2015-208032.

53. Su, Q., Yao, J., and Sheng, C. (2018). Geniposide Attenuates LPS-Induced Injury via Up-Regulation of miR-145 in H9c2 Cells. Inflammation *41*, 1229–1237. https://doi.org/10.1007/s10753-018-0769-8.

54. Wang, J., Xu, X., Li, P., Zhang, B., and Zhang, J. (2021). HDAC3 protects against atherosclerosis through inhibition of inflammation via the microRNA-19b/PPARγ/NF-κB axis. Atherosclerosis *323*, 1–12. https://doi.org/10.1016/j.atherosclerosis.2021.02.013.

55. Wang, Q., Liu, J., Hu, Y., Pan, T., Xu, Y., Yu, J., Xiong, W., Zhou, Q., and Wang, Y. (2021). Local administration of liposomal-based Srpx2 gene therapy reverses pulmonary fibrosis by blockading fibroblast-to-myofibroblast transition. Theranostics *11*, 7110–7125. https://doi.org/10.7150/thno.61085.

STAR★METHODS

KEY RESOURCES TABLE

REAGENT or RESOURCE	SOURCE	IDENTIFIER
Antibodies		
HDAC3	Abcam	Cat#ab137704
GAPDH	Abcam	Cat#ab8245
β-Actin	Abcam	Cat#ab8226
GSDMD-N	Abcam	Cat#ab210070, ab209845
CD68	Cell Signaling Technology (CST)	Cat#29176
cGAS	CST	Cat#79978,31659
NLRP3	CST	Cat#15101
phosphorylated (P)-STING	Abcam	Cat#50907,72971
total (T)-STING	Abcam	Cat#13647
IL-6	Abclonal	Cat#A0286
Caspase-1 p20	Abclonal	Cat#A0964
H3K9Ac	Abclonal	Cat#A7255
H3	Abclonal	Cat#A2348
Horseradish peroxidase (HRP)-coupled goat anti-mouse/rabbit IgG	Abclonal	Cat#AS063, AS064
Alexa Fluor 488- and 568-conjugated secondary antibodies	Abclonal	Cat#A-11008,A-11001,A-110011, A11004
Chemicals, Peptides, and Recombinant Proteins		
DAPI	Sigma	Cat#S7113
PI	Beyotime	Cat#ST511
Hoechst 33258	Beyotime	Cat#C1018
3-MA	MCE	Cat#HY-19312
MG132	MCE	Cat#HY-13259
Tamoxifen	Sigma	Cat#T5648
FBS	Gibco	Cat#10099-141
RPMI-1640	Gibco	Cat# 11875119
DMEM	Gibco	Cat#11965092
LPS	Sigma	Cat#L2630
PMA	MCE	Cat#HY-18739
mPEG2000-DMG	MCE	Cat#HY-112764
Other		
Cell counting kit-8	AbMole	Cat# M4839
Proteasomal activity detecting kits	UBPBio	Cat# G2100, G1100, G3100
TNF-α ELISA kits	Abcam	Cat# ab285312, ab208348
IL-1β ELISA kits	Abcam	Cat#ab214025, ab197742
IL-18 ELISA kits	Abcam	Cat#ab240391, ab207323
HMGB1 ELISA kits	ARGIO	Cat# ARG81351
Experimental Models: Cell Lines		
THP-1 cells	CCLB	N/A

(*Continued on next page*)

Continued

REAGENT or RESOURCE	SOURCE	IDENTIFIER
Experimental Models: Organisms/Strains		
C57BL/6 mice	Institute of Laboratory Animal Science, Chinese Academy of Medical Sciences	N/A
HDAC3$^{flox/flox}$ mice	Shanghai Model Organisms Center	N/A
Lyz2-CreERT2 transgenic mice		Cat#T052789
Oligonucleotides		
See Table S1	This paper	N/A

RESOURCE AVAILABILITY

Lead contact

Further information and requests for resources and reagents should be directed to and will be fulfilled by the lead contact, Qing Geng (gengqingwhu@whu.edu.cn).

Materials availability

This study did not generate new unique reagents.

Data and code availability

- All data reported in this paper will be shared by the lead contact upon request.
- This paper does not report original code.
- Any additional information required to reanalyze the data reported in this paper is available from the lead contact upon request.

EXPERIMENTAL MODEL AND SUBJECT DETAILS

Animals and treatment

All animal experiments in this study were approved by the Animal Care and Use Committee of Wuhan university and carried out on the basis of the Guidelines for Care and Use of Laboratory Animals published by the US National Institutes of Health (NIH Publication No. 85-23, revised 1996). The mice were kept in the Animal Center of Wuhan university in a specific pathogen-free (SPF) barrier system with a humidity of 45–55% and a temperature of 20–25°C on a regular 12 h light/dark cycle. Wild type male C57BL/6 mice (8–10 weeks old, 23.1–25.8 g) were obtained from the Institute of Laboratory Animal Science, Chinese Academy of Medical Sciences (Beijing, China). HDAC3$^{flox/flox}$ mice were generated via the CRISPR-Cas9 system by the Shanghai Model Organisms Center, Inc. The tamoxifen-inducible Lyz2-CreERT2 transgenic mice with C57BL/6 background were also purchased from GemPharmatech (Nanjing, China). As shown in Figure 3A, the LoxP sequences were inserted in the introns flanked with the exon 4 to 7 of HDAC3. To generate macrophage HDAC3-deficient (HDAC3 CKO) mice, the Lyz2-CreERT2^{+}mice were crossed with HDAC3$^{flox/flox}$ mice. The Lyz2-CreERT2^{-}-HDAC3$^{flox/flox}$ (HDAC3-C) mice from littermates were used to be controls. Male mice (8–10 weeks old) were treated with tamoxifen (10 mg/kg) dissolved in corn oil intraperitoneally for five consecutive days before experiments. To establish an *in vivo* ALI model, the mice were intraperitoneally injected with LPS (10 mg/kg) dissolved in 50 μL sterile saline, as previously reported.[11] To upregulate miR-4767 *in vivo*, mice were pretreated with miR-4767 antagomir (80 mg/kg/day) or antagomir negative control (Antagomir NC) via tail vein injection for 3 days before LPS stimulation. Additionally, *Hdac3* siRNA-loaded liposomes or scrambled siRNA-loaded liposomes were intratracheally injected into the mice 36 hours before LPS stimulation. Under deep anesthesia (0.3% pentobarbital sodium injected intraperitoneally, 0.1 ml/10 g), the mice were sacrificed by cervical dislocation after LPS injection for 12 hours. Subsequently, the intact left lungs were excised and instilled with neutral buffered formalin (10%) to maintain the alveoli in an intumescent status. The right lungs were rapidly cut into pieces and stored in liquid nitrogen for subsequent analysis.

Cell culture and treatment

The hominine monocytic THP-1 cells were purchased from the China Cell Line Bank (Beijing, China). The THP-1 cells were cultured in RPIM-1640 medium containing fetal bovine serum (10%). Phorbol

12-myristate 13-acetate (100 ng/ml) was added to the medium for 12 hours to induce the differentiation of THP-1 cells into adherent macrophages. To downregulate HDAC3, the differentiated THP-1 cells were infected with siRNA (GenePharma Co., Ltd., Shanghai, China). On the basis of the manufacturer's instructions, the differentiated THP-1 cells were incubated with Lipofectamine™ 3000 Transfection Reagent (Thermo Fisher Scientific, Waltham, MA, USA) before siRNA transfection. To overexpress HDAC3, the THP-1 cells were transduced with Ad-*Hdac3* (MOI = 100) or adenovirus harboring no overexpression sequence (vehicle) for 24 hours. To overexpress cGAS, the THP-1 cells were transduced with Ad-*cGAS* (MOI = 30) or adenovirus harboring no overexpression sequence (vehicle) for 12 hours. The study employed MG132 (20 μM) to inhibit proteasome function and 3-MA (5 μM) to suppress autophagy.[45] To induce pyroptosis in macrophages, the cells were stimulated with LPS (1 μg/mL) for 4 hours, followed with the incubation with nigericin (10 μM) for 0.5 hour.[46] The THP-1 cells were transfected with miR-4767 antagomir (50 nmol/L), agomir (50 nmol/L), or the negative controls synthesized by Ribobio Inc. (Guangzhou, China) using Lipofectamine™ 3000 Transfection Reagent as described.[47]

Primary macrophages were obtained by using DMEM medium without serum to lavage the peritoneal cavity of mice that had been intraperitoneally injected with DMEM 3 days in advance, as described in a previous study.[48] The obtained primary macrophages were cultured in DMEM medium containing fetal bovine serum (10%) for subsequent experiments.

METHOD DETAILS

Histopathological analysis

Hematoxylin&eosin (H&E) staining was performed to assess the degree of lung pathological injury.

Briefly, the left lung tissues were fixed with neutral buffered formalin (10%) and then embedded in paraffin. Next, the lung tissue wax blocks were transversely cut into 3-μm-sections and stained with H&E to observe neutrophil infiltration and pulmonary edema. A semi-quantitative scoring system was employed to evaluate lung injury on the basis of the degree of neutrophil infiltration and pulmonary edema. For each index, a 5-point scale was applied: 0, minimal damage; 1 to >2, mild damage; 2 to >3, moderate damage; 3 to >4, severe damage; and 4+, maximal damage. The total lung injury score was determined as the sum of the neutrophil infiltration score as well as the pulmonary edema score, as described previously.[49]

Immunofluorescence staining was performed to detect HDAC3 and CD68 in the murine lung tissue, and HDAC3 in the THP-1 cells.[38] The lung tissue sections were deparaffinized and the antigen was retrieved in citric acid buffer under high temperature. Subsequently, the sections were incubated with the primary antibodies against CD68 and HDAC3 at 4°C overnight. The next day, the sections were incubated with Alexa Fluor 568 (Red) or Alexa Fluor 488 (Green)-conjugated secondary antibodies for 1 h at 37°C away from light. DAPI was used to stain cell nuclei as blue. Finally, the DX51 fluorescence microscope (Olympus, Japan) was used to observe and capture the immunofluorescence images.

Real-time PCR and western blot

The total RNA was isolated from the frozen lung tissues or the THP-1 cells using TRIzol reagent.

Then the concentration and purity of RNA dissolved with 20 μL of DEPC water was measured by a spectrophotometer. After the RNA was reversed into cDNA with a reverse transcription kit, the expression levels of related mRNAs were quantified with SYBR Green Real-time PCR Master Mix and analyzed using $2^{-\Delta\Delta Ct}$ method with an internal reference gene *Gapdh* or *U6*.[50] The information of primers used in the present study was displayed in Table S1.

Prepared cell samples or freeze-ground lung tissues were resuspended with protease inhibitor (PMSF)-containing RIPA lysate and lysed on ice for 30 min, followed by the unification of the total protein concentration of each sample according to the BCA method. Samples were added to the SDS-PAGE gels at appropriate concentrations for electrophoresis and transferred to PVDF membranes. After sealing the membrane containing the separated protein samples with BSA (5%), the specific primary antibodies were incubated at 4°C overnight. The next day, the blots were incubated with the secondary antibodies at room temperature. The relative protein expression was detected via chemiluminescence and the gray value of protein expression was analyzed using ImageJ software as described[51]

PI-Hoechst staining

To begin with, the THP-1 cell samples were washed with pre-cooled phosphate-buffered saline (PBS) for 3 times. Then the samples were fixed with paraformaldehyde (4%) and stained with PI and Hoechst for 10 min. Finally, cells were observed and photographed under a fluorescence microscopy away from light.

The determination of HMGB1, IL-1β, IL-18 and TNF-α

The cell supernatant from cultured cells and the homogenate of lung tissues were collected and centrifuged. As reported in previous studies, samples of bronchial lavage fluid (BALF) were obtained by repeated gentle rinsing of the mouse bronchus three times with 500μL 0.9% saline that had been precooled in advance.[52] Then the concentrations of inflammatory cytokines were detected using commercial ELISA Assay kits as described.[13] The absorbance was tested using a microplate reader.

Cell viability

The CCK-8 Assay kit was used to measure cell viability in the THP-1 cell after LPS and nigericin stimulation based on the instructions from one previous study.[53]

The detection of mitochondrial DNA in cytoplasm

The level of mitochondrial DNA (mt-DNA) was detected using the Mitochondrial DNA Isolation Kit purchased from Abcam (Cambridge, UK). The THP-1 cells were then lysed and centrifuged (x 700 g) at 4°C for 10 min to obtain the supernate, followed by the centrifugation (x 10 000g) at 4°C for 30 min. According to the principle of differential centrifugation, mt-DNA in mitochondria existed in sediment while mt-DNA in cytoplasm existed in supernate. The relative level of mt-DNA in cytoplasm was reflected by cytochrome *c* oxidase III via Real-time PCR and 18S was used as an internal reference gene.

Proteasomal activity

In brief, the cultured THP-1 cells were pretreated with the ice-cold cell lysis buffer without detergents or protease inhibitors. Then the cell lysis buffer was centrifuged (x 17, 000 g) at 4°C for 20 min. And the supernate was used to detect protein concentration as well as proteasomal activities. Caspase-like, chemotrypsin-like, and trypsin-like activities were detected by the following synthetic fluorogenic peptides: Z-Leu-Leu-Glu-AMC, Suc-Leu-Leu-Val-Tyr-AMC, and Boc-Leu-Arg-Arg-AMC at excitation/emission wavelength of 380 nm/460 nm.

Dual-luciferase reporter gene assay

3′UTR: 1017–1023, h-cGAS-WT (CGCCCGC) and h-cGAS-WT (GCGGGCG).

The wild type and mutant type sequences of h-cGAS-WT (CGCCCGC) and h-cGAS-MUT (GCGGGCG) at 3′UTR from 1017 to 1023 were synthesized artificially, and cloned into the pMIR-reporter on the basis of the instructions of luciferase assay kit. Subsequently, cGAS-3′UTR-WT as well as cGAS-3′UTR-MUT were co-transfected with agomir NC vector or agomir miR-4767 vector into THP-1 cells. After transfection for 48 h, the luciferase activity was detected through a dual-luciferase system according to the previous protocol. miR-4767 gene was then digested by restriction endonuclease, the promoter fragment of which was inserted into the pGL3-basic reporter plasmid. Finally, the luciferase activity was detected via a Glomax20/20 luminometer using a luciferase assay kit as described.[54]

Chromatin immunoprecipitation (CHIP)

THP-1 cells were transduced with Ad-*Hdac3* or transfected with *Hadc3* siRNA, which were then fixed with formaldehyde (4%) for 10 min to form DNA-protein crosslinks. Glycine (2 mg/mL) was utilized to neutralize superfluous paraformaldehyde. Cells were disrupted using an ultrasonic disruptor followed by centrifugation at 12000*g* for 3min. Anti-HDAC3 antibody and negative control normal mouse IgG antibody were added into the supernatant. After that, Protein Agarose/Sepharose was used to precipitate the DNA-protein complexes by centrifuging at 12000g, followed by the extraction and purification of the DNA fragments. Finally, the binding of HDAC3 to miR-4767 promoter was determined via real-time quantitative PCR.

Preparation and characterization of *Hdac3* siRNA-loaded liposomes

Hdac3 siRNA-loaded liposomes were constructed as reported.[55] In brief, the siRNA was dissolved in citrate buffer (10 mM, pH = 3) and rapidly mixed with a lipid mixture by vortexing. Distearoyl phosphatidylcholine

(DSPC), lipidoid, 1,2-dimyristoyl-rac-*glycero*-3-methoxypolyethylene glycol-2000 (mPEG-DMG), as well as cholesterol were dissolved in ethanol at a molar ratio of 38.5:50:1.5:10. *Hdac3* siRNA or scrambled siRNA was dissolved in citrated buffer (10 mM, pH 3), followed by the blending with a lipid mixture. The unentrapped siRNA was then excluded by ultrafiltration centrifugation. Last, the siRNA-loaded liposomes were diluted in PBS. The characteristics of liposomes involving morphology, zeta potential, hydrodynamic diameter, polydispersity, and stability were detected via dynamic light scattering. Additionally, the entrapment efficiency was detected using RiboGreen assay. The liposomes were characterized by transmission electron microscopy after stained with phosphotungstic acid (2%).

Statistical analysis

All the data in this study were expressed as the mean ± standard error of the mean (SEM) and analyzed using the SPSS 23.0 software. Unpaired Student's *t* test was used for comparisons between two groups. Two-way analysis of variance (ANOVA) without repeated measures was performed for multiple comparisons with two independent variables. One-way ANOVA with Tukeys post hoc test was used for comparisons among three or more groups. Tukey's tests were run only when F achieved $p < 0.05$, and no significant variance inhomogeneity was found; otherwise, Tamhane's T2 post hoc test was performed. Normality and homogeneity were tested using Liljefors' and Levene's tests, respectively. Statistical significance was set at $p < 0.05$.